PREDICTION OF MECHANICAL, ELECTRIC, AND THERMAL PROPERTIES OF COPPER ALLOYS BASED ON COMPOSITION AND PROCESSING USING MACHINE LEARNING

Jaka Fajar Fatriansyah, Yossi Andreano
Department of Metallurgical and Materials Engineering

INTRODUCTION

Problems

- The application of **leadframes** requires a complex set of specifications, including **high strength**, **high conductivity**, and **low thermal expansion coefficient** to ensure optimal performance.
- **Discovering copper materials** that achieve this combination of properties through **experimental method** involves **significant costs** and is **time-consuming**.

Objective

Develop ML models for **predicting** and **reverse-predicting** the tensile strength, electrical conductivity, and thermal expansion coefficient of copper alloys based on their chemical composition and processing methods and to **assess the performance** of these models in **selecting optimal copper alloy materials**.

METHODOLOGY

Machine Learning Modelling

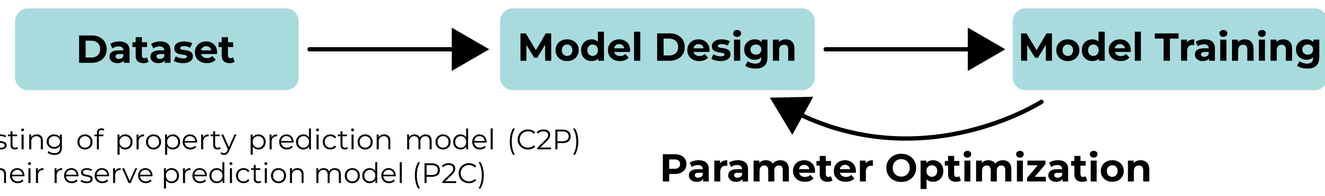

* Consisting of property prediction model (C2P) and their reserve prediction model (P2C)

Machine Learning Design System (MLDS)

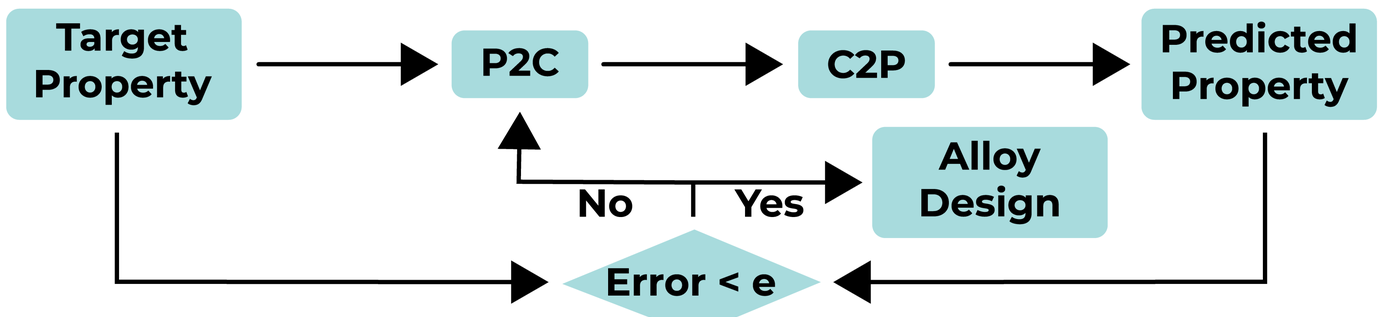

RESULT

- **From the six trained models** (KNN, RF, ExtraTrees, Catboost, XGB, and BPNN), the two **best C2P and P2C** models obtained are **BPNN** and **XGB** as shown in Figure 1.
- **MLDS XGB** shows **lower fluctuations** compared to **MLDS BPNN** and **P2C BPNN** in providing recommendations for copper alloy composition and processing, spesifically referencing **C41300** material as shown in Figure 2.
- **MLDS XGB** can be used to **recommend new copper alloys** for leadframe applications that are **in line** with the **literature** as shown in Table 1.

Fig 1. The performance of the best C2P and P2C models

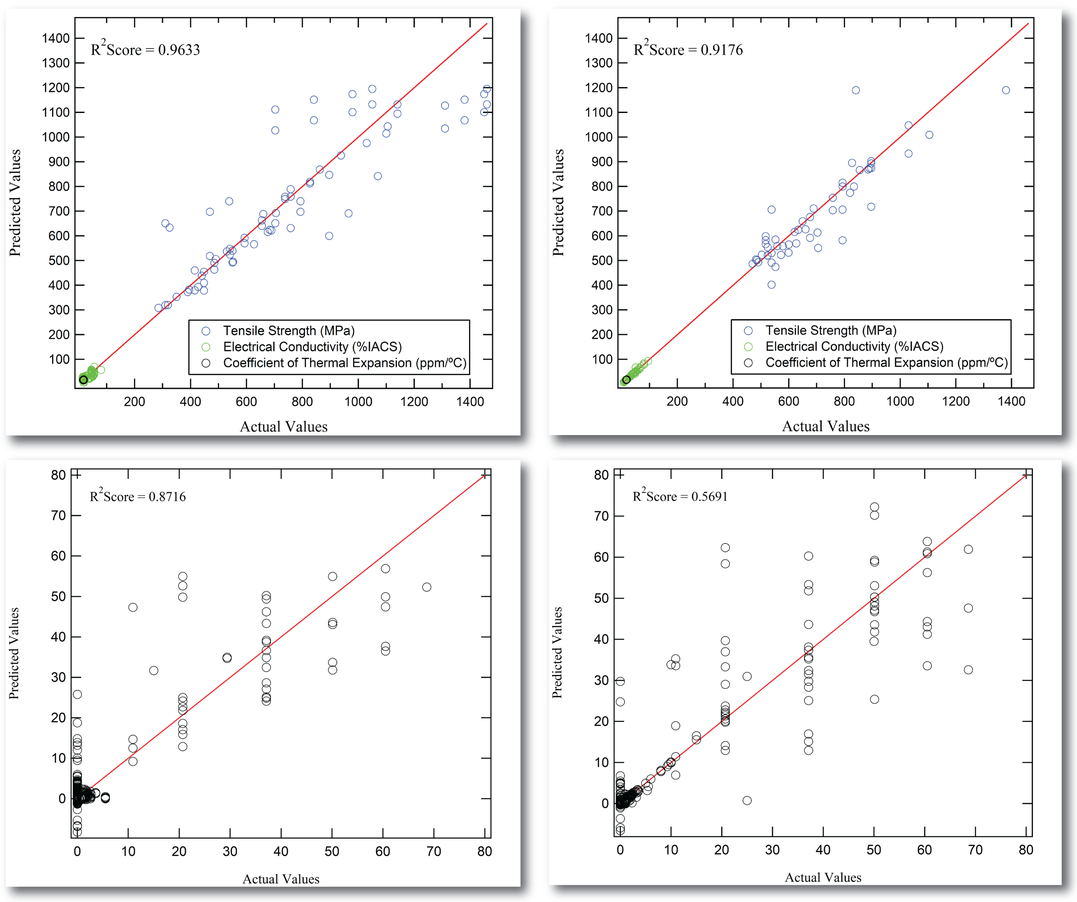

Fig 2. Main elements (Zn and Sn) of alloy designed by MLDS and P2C models

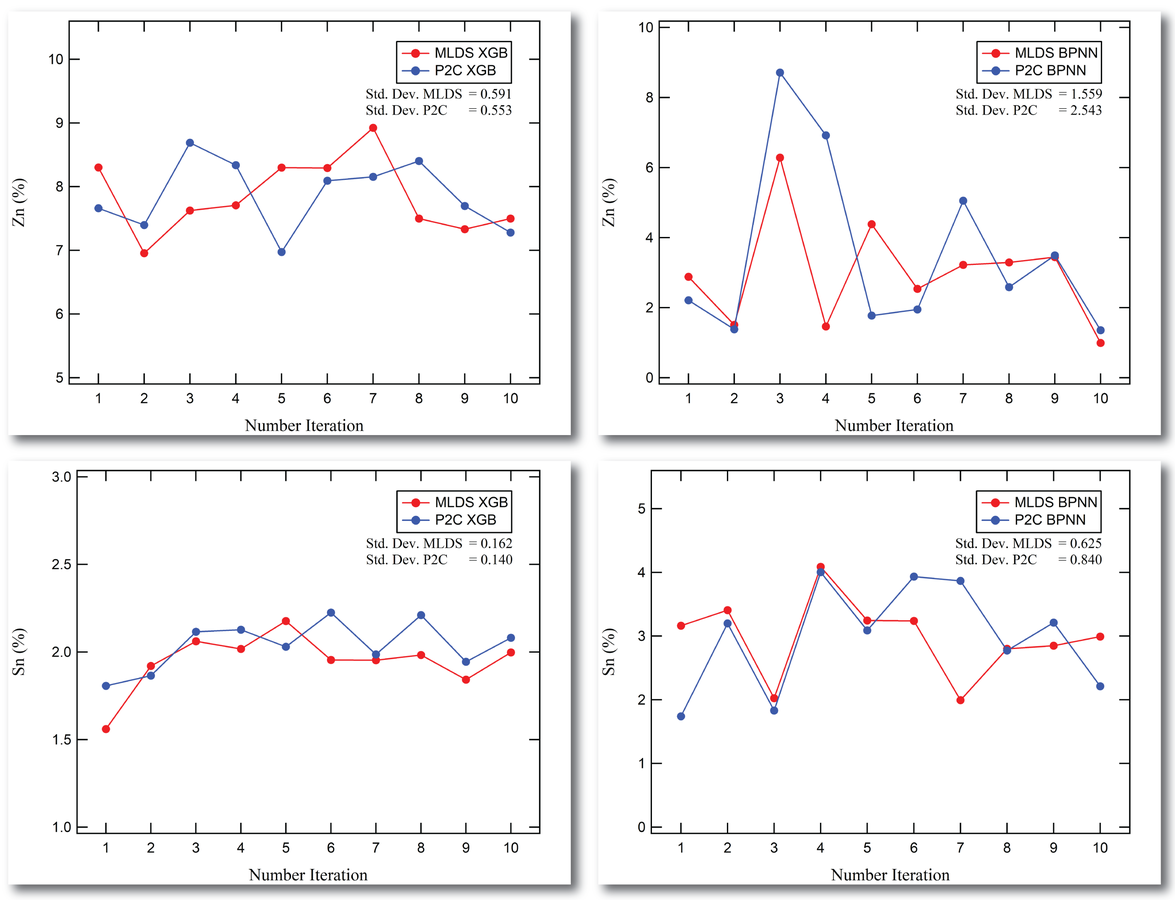

Table 1. Design Result and Verification

Target	MLDS Result	Experimental Design	Experimental Result
575 MPa 85% IACS 17 ppm/°C	● Cu-0.21Fe-0.16Zr-0.52Cr-0.03Ti-0.04Ag (C) ● Solution treatment, 45% CR, and aging (P)	● Cu-0.15Zr-0.5Cr-0.1Ag (C) ● Solution treatment, 80% CR, and aging (P)	570 MPa 86% IACS

CONCLUSION

BPNN and XGB are the **two best models** for C2P and P2C, but the **performance of MLDS XGB** in recommending copper alloy composition and processing is **significantly better**.

Complexity, Fluctuations and Dissipation in Nonlinear, Non-equilibrium models

ATHOKPAM Langlen Chanu
Asia Pacific Center for Theoretical Physics, Pohang, South Korea

(A) Simple oscillations (spiking) (B) Complex oscillations (bursting)

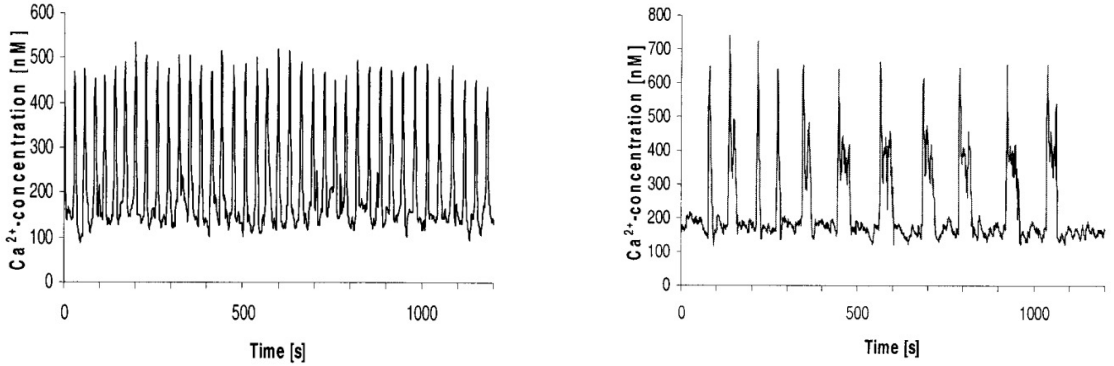

Rat hepatocytes stimulated with (A) 2μM phenylephrine, (B) 1.2 μM ATP

Stochastic modelling with Chemical Langevin Equation:

System size (V)

Intrinsic fluctuation $\sim \dfrac{1}{\sqrt{V}}$

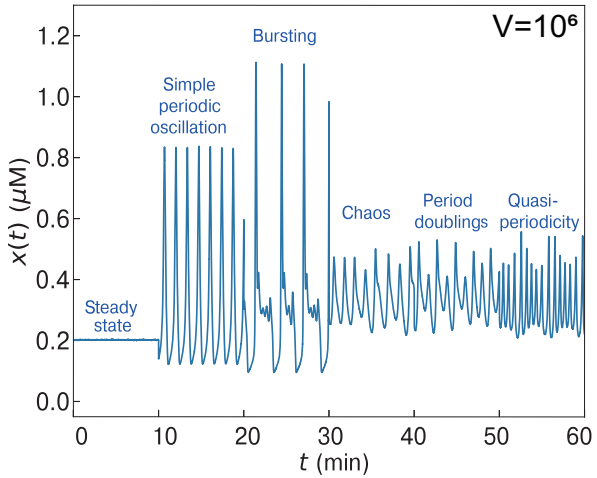

Intracellular Calcium (Ca^{2+}) dynamics

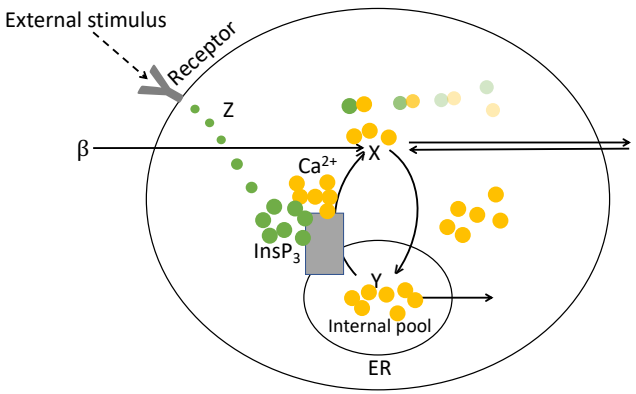

Coupled, non-linear ODEs

$$\frac{dx}{dt} = V_0 + V_1\beta - V_2 + V_3 + k_f y - kx$$

$$\frac{dy}{dt} = V_2 - V_3 - k_f y$$

$$\frac{dz}{dt} = \beta V_4 - V_5 - \epsilon z$$

$$V_2 = V_{M2}\frac{x^2}{K_2^2 + x^2}$$

$$V_3 = V_{M3}\frac{x^m}{K_x^m + x^m}\frac{y^2}{K_y^2 + y^2}\frac{z^4}{K_z^4 + z^4}$$

$$V_5 = V_{M5}\frac{z^p}{K_5^p + z^p}\frac{x^n}{K_d^n + x^n}$$

How do intrinsic fluctuations interact with the "complexity" of intracellular Ca^{2+} dynamics?

- Permutation Entropy
- Statistical Complexity

Kummer, U., *et al.* (2000). *Biophysical journal*, ***79***(3), 1188-1195.
Houart, G., Dupont, G., & Goldbeter, A. (1999). *Bulletin of mathematical biology*, ***61***(3), 507-530.
Gillespie, D. T. (2000). *The Journal of Chemical Physics*, ***113***(1), 297-306.

Regular (Periodic)

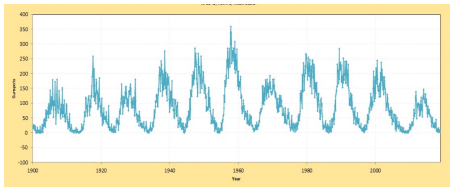

Chaotic

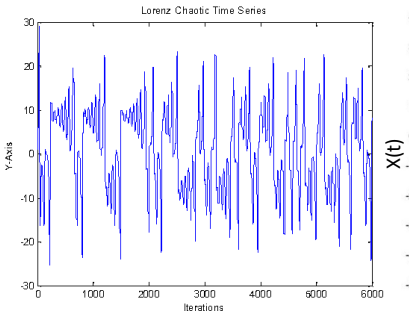

Random

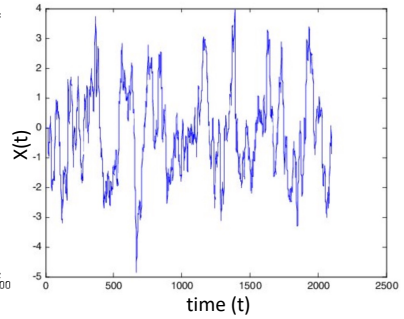

Permutation Entropy - a complexity measure for time series

$$S[P] = -\sum_{j=1}^{r!} \rho_j(\pi_j) \log \rho_j(\pi_j)$$

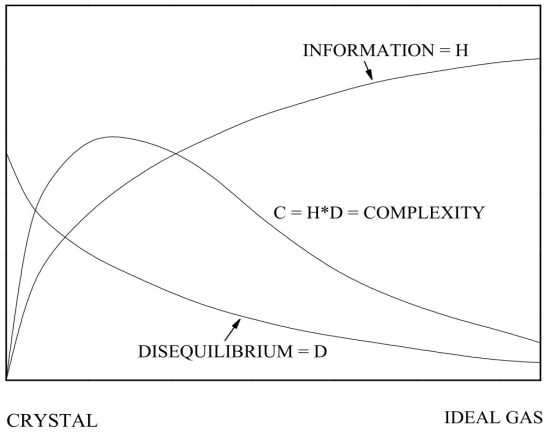

Statistical Complexity

Complexity-Entropy Plane

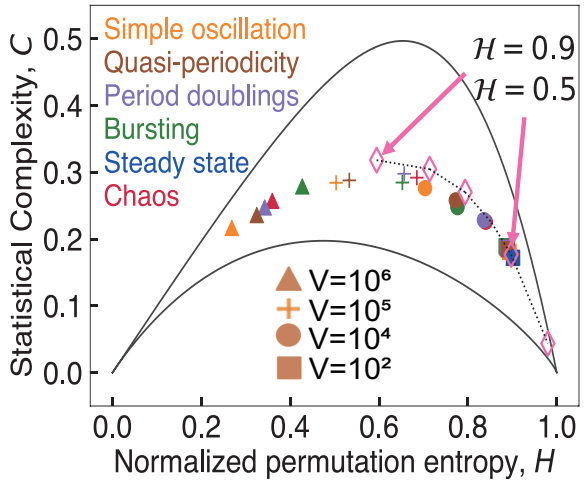

Non-Equilibrium Chemical Reaction System

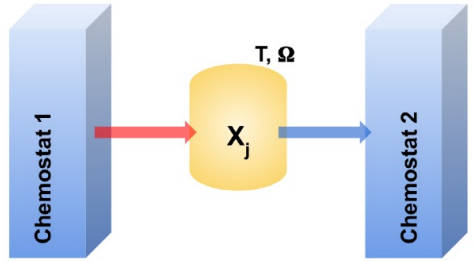

(a) Intracellular Ca^{2+} oscillation

(b) Hindmarsh-Rose neuron model

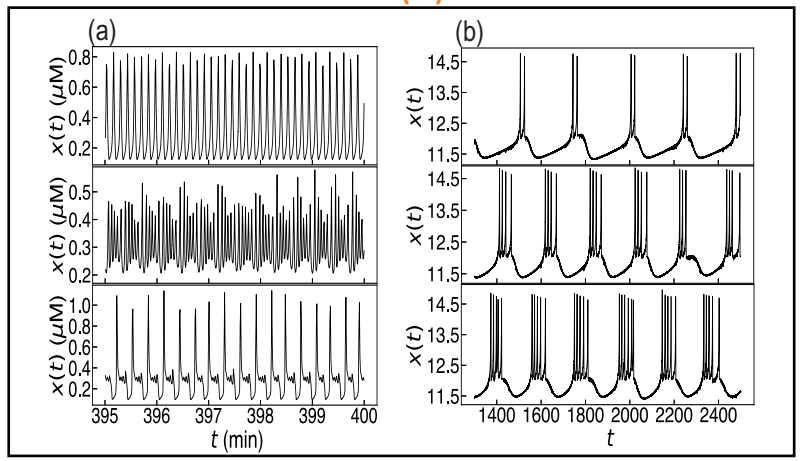

Chemical Langevin Equation: $d\mathbf{x} = \boldsymbol{F}(\mathbf{x})dt + \frac{1}{\sqrt{\Omega}}\boldsymbol{G}(\mathbf{x})d\boldsymbol{W}$

Stochastic thermodynamics

- Non-Equilibrium Steady State
- Total Entropy Production Rate

Investigate dissipation in stochastic complex oscillations

Poster #3

Bandt, C., & Pompe, B. (2002) *Physical review letters*, ***88***(17), 174102.
Lopez-Ruiz, R., Mancini, H. L., & Calbet, X. (1995). *Physics letters A*, ***209***(5-6), 321-326.
Chanu, A.L., Singh, R.K.B., Jeon, & J.-H. (2024) *Chaos, Solitons & Fractals*, **185**, 115138.
Chanu, A.L., Mishra, P., Kumar, S., & Singh, R.K.B. (2024) *arXiv preprint arXiv:2406.06019*.

Skin effect and the bulk-boundary correspondence

Hatano-Nelson model

$$H = \sum_{n=1}^{L-1} \left(t_R c_{n+1}^\dagger c_n + t_L c_n^\dagger c_{n+1} \right)$$

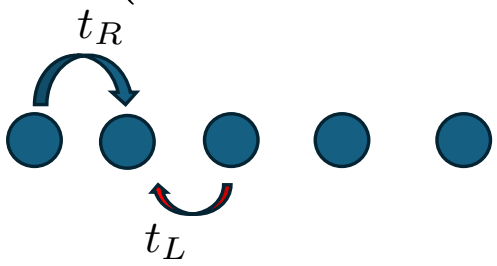

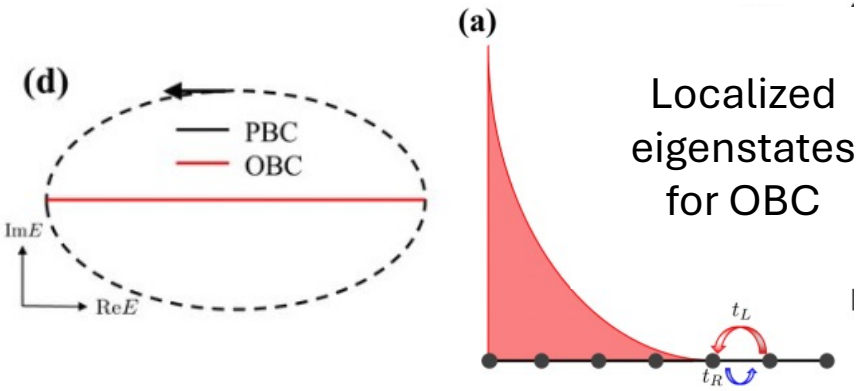

Localized eigenstates for OBC

SSH model

$$H_{\text{targ}}^{\text{SSH}} = \sum_j \left(t_1 c_{A,j}^\dagger c_{B,j} + t_2 c_{B,j}^\dagger c_{A,j+1} + h.c. \right)$$

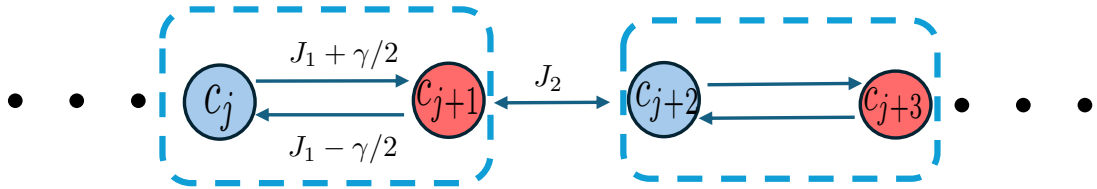

OBC spectrum

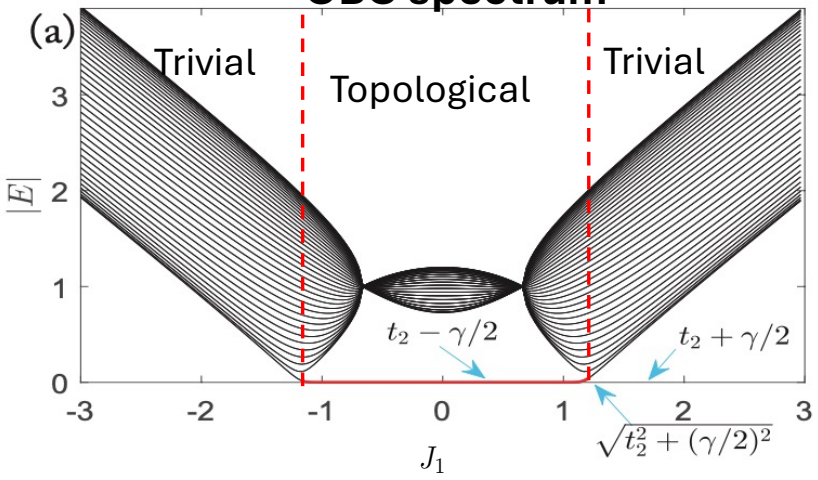

Zero energy for PBC!

Shunyu Yao and Zhong Wang Phys. Rev. Lett. **121**, 086803 (2018).

Numerics

(a) $t = 0$

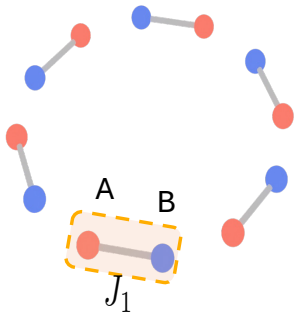

$t > 0$

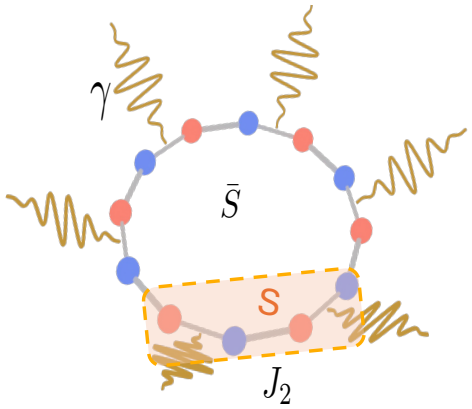

(b) Phase diagram

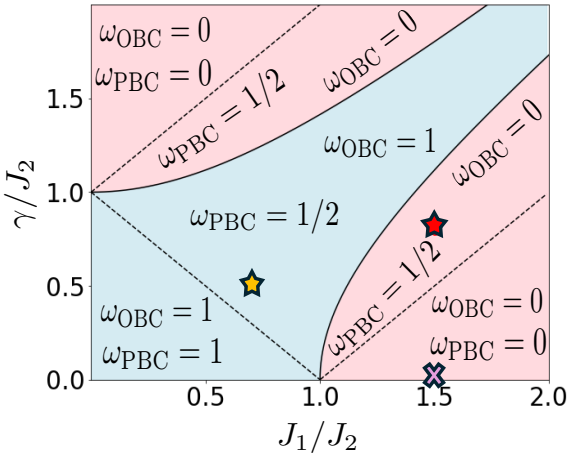

$$C_{mn} : \mathrm{Tr}[\rho(t) c_n^\dagger c_m]$$

$$\xi_k = \frac{1}{e^{\epsilon_k} + 1}$$

(c) Trivial to topological

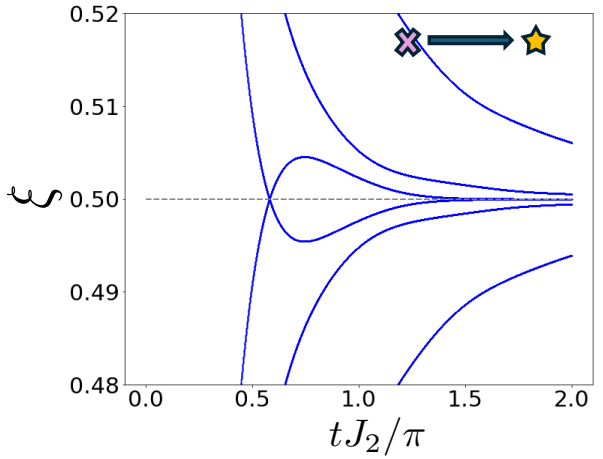

(d) Trivial to trivial

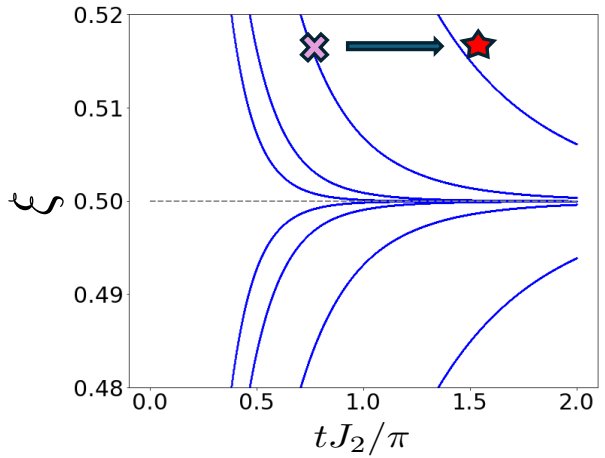

Machine Learning Utilization to Predict Quinazoline Derivatives as Hepatitis B Virus Inhibitors

Jaka Fajar Fatriansyah[1], Anggit Driasaditya[2]
Departemen of Metallurgical and Materials Engineering
Universitas Indonesia

UNIVERSITAS INDONESIA
Veritas, Probitas, Iustitia
FAKULTAS TEKNIK

BACKGROUND

Liver cancer, especially hepatocellular carcinoma (HCC), is an increasing global health challenge, with more than 1 million new cases estimated annually by 2025. Hepatitis B virus (HBV) is a major risk factor for the development of HCC, accounting for approximately 50% of total cases.

In Indonesia, the prevalence of chronic HBV infection is very high, making it one of the countries with the highest number of patients in Asia. One of the mechanism of HCC development involves protein signaling pathways such as VEGFR-2, which is often the target of antiangiogenic treatment.

GOALS

This study aims to evaluate the interaction of quinazoline compounds with VEGFR-2 receptors using in silico and machine learning approaches to accelerate the drug discovery process. The ML models used to improve the efficiency of predicting the tethering value are K-Nearest Neighbor, Extra Trees, Extreme Gradient Boosting, and Artificial Neural Network.

Two types of input data were compared: SMILES, which represents the molecular structure linearly, and AlvaDesc descriptors, which provide physicochemical information and also determine the most effective input method to predict the tetheringh score of quinazoline's compounds on VEGFR-2 DNA targets, so as to optimize the drug discovery process with higher time and cost efficiency.

METHODS

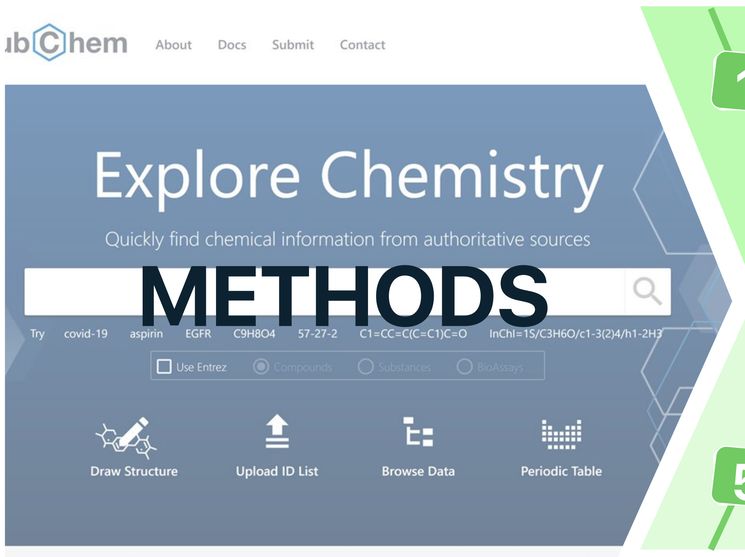

1. Collecting the quinazoline's derivative compounds from PubChem website using the substructure option
2. Molecular docking study to investigate compounds and protein target relative binding affinities and binding interactions. Docking study was performed using AutoDock Vina.
3. Creating a new dataset as an input which consist of affinity, compound id, and descriptors.
4. SMILES and Alvadesc are used as descriptors, where SMILES is converted by one-hot coding and Alvadesc is obtained through its software to obtain the descriptor.
5. The 4 model of machine learning utilized the descriptor that used to predict the docking score

KNN

Uses the number of nearest data points (K) to predict characteristics, influenced by the closest neighbors.

ANN

Uses neurons in multiple layers to predict outcomes, with tunable hyperparameters like batch size, epoch, learning rate, activation function, optimizer, and network structure.

XTRATREE

A decision tree algorithm that selects split points randomly from a subset of features to enhance randomness and model performance.

XGB

An advanced version of random forest and gradient boosting, designed for faster computation and higher accuracy. Applicable for regression and classification. of the model. XG Boost can be used for regression or classification problems.

RESULT

1. Model comparison using Alvadesc descriptors

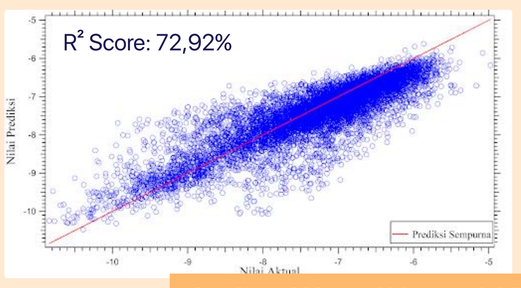

Artifiicial Neural Network/ ANN

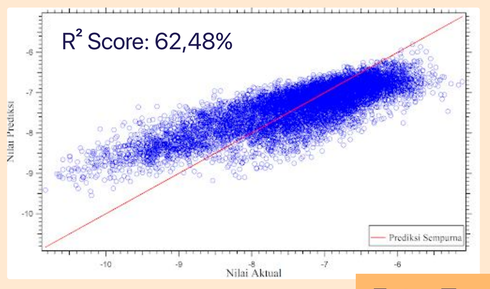

Extra Trees

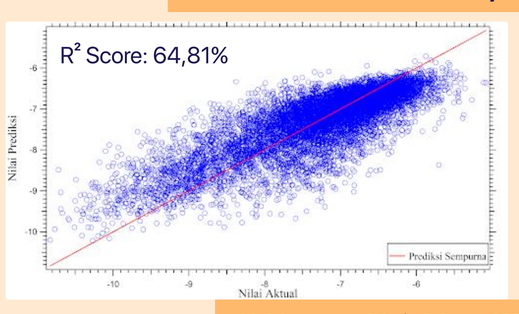

K-Nearest Neighbor / KNN

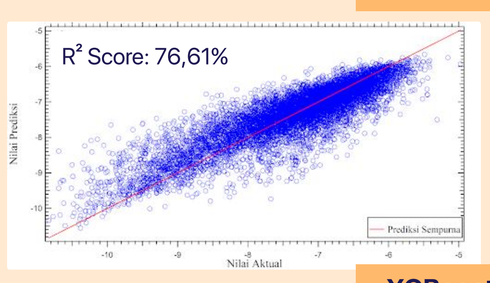

XGBoost

2. Feature Importance

Feature	Importance	Correlation
F01 [C-C]	0.10253943	-0.634501714
nCsp2	0.02967717	-0.596003663
P1v	0.02392009	-0.461895856
CATS2D 02 DA	0.01502753	-0.166060624
R6v	0.01141004	0.103887489

F01[C-C]

This descriptor measures the number of inter-carbon bonds (adjacent carbons) in a molecule, indicating the frequency of direct bonds between carbon atoms.

F01[C-C] has a clear correlation with the docking value; the higher the F01[C-C] variable, the better the docking value. This is consistent with Pearson correlation analysis, which shows a large absolute value.

STUDY CASE

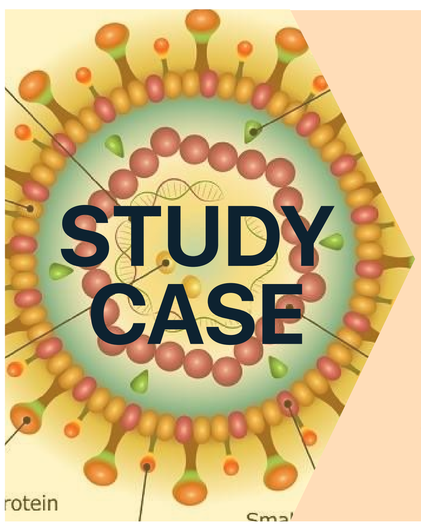

Compound	Actual Score	Predict Score	IC_{50}(nM)	F01 [C-C]
Quinazoline	-5,796	-6,639	16,6	7
Sorafenib	-6,336	-7,193	2,4	18
Lenvatinib	-9,302	-7,165	4	19
Axitinib	-10,790	-7,157	0.25	21

The study case suggests that there is an inverse relationship between the actual score and the F01[C-C] value. Higher F01[C-C] values, are associated with lower (more negative) actual scores. This imply that molecules with more inter-carbon bonds tend to have better binding affinities (lower actual scores).

CONCLUSION

Accurate predictions of molecular tethering values were achieved using three machine learning models: K-Nearest Neighbor (64.81%), Extra Trees (62.48%), and Extreme Gradient Boosting (76.6%), as well as a deep learning model: Artificial Neural Network (72.96%). The XGB model produced the highest accuracy.

Quantum jumps in driven-dissipative disordered many-body systems

Sparsh Gupta

In collaboration with Hari Kumar Yadalam, Manas Kulkarni and Camille Aron

Phys. Rev. A 109, L050201 (2024)

Dynamics Days Asia Pacific 13
Yukawa Institute for Theoretical Physics, Kyoto University, Japan
July 1st — 5th, 2024

Setup

- Deformed Lindblad Equation:

$$\frac{d}{dt}\rho(t) = \mathcal{L}_\zeta \rho(t), \tag{1}$$

where the ζ-deformed Liouvillian is

$$\mathcal{L}_\zeta \star = -\mathrm{i}\,[H, \star] + \sum_{\alpha=1}^{M} \left[\zeta O_\alpha \star O_\alpha^\dagger - \frac{1}{2} \left\{ O_\alpha^\dagger O_\alpha, \star \right\} \right] \tag{2}$$

$$H = \sum_{i=1}^{L} h_i n_i - J \sum_{i=1}^{L-1} \left(b_i^\dagger b_{i+1} + \mathrm{H.c.} \right) + U \sum_{i=1}^{L-1} n_i n_{i+1}, \tag{3}$$

$$O_i = \begin{cases} \sqrt{2\gamma}\; b_i^\dagger & \text{if } i \text{ is odd} \\ \sqrt{2\gamma}\; b_i & \text{if } i \text{ is even}\,. \end{cases} \tag{4}$$

- Trace Preserving Evolution equation for density matrix $\rho_\zeta(t)$:

$$\partial_t \rho_\zeta(t) = \left(\mathcal{L}_\zeta - \mathrm{Tr}\left[\mathcal{L}_\zeta \rho_\zeta(t) \right] \right) \rho_\zeta(t)\,. \tag{5}$$

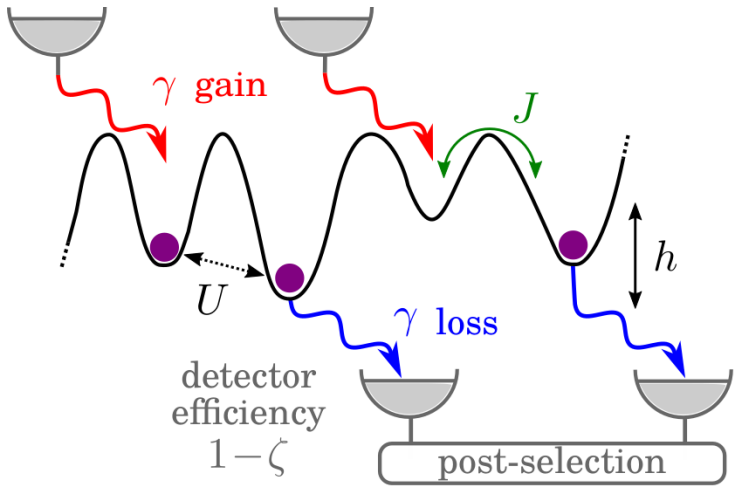

Disordered gain-loss model with hardcore bosons.

Results

Initial state $\rho(0) = |1, 0, \cdots, 1, 0\rangle\langle 1, 0, \cdots, 1, 0|$

Complex Spacing Ratios

$$\xi_k = \frac{z_k^{NN} - z_k}{z_k^{NNN} - z_k} = r_k e^{i\theta_k},$$

Imbalance

$$\mathcal{I}(t) = \frac{N_O - N_E}{N_O + N_E},$$

Rate of Dynamical Activity

$$\dot{\mathcal{A}}(t) = \frac{1}{\zeta}\partial_t \langle n(t)\rangle_\zeta \tag{6}$$

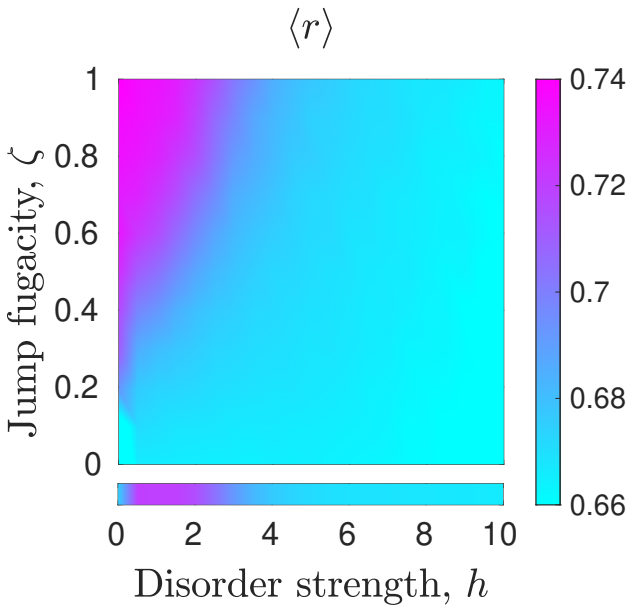

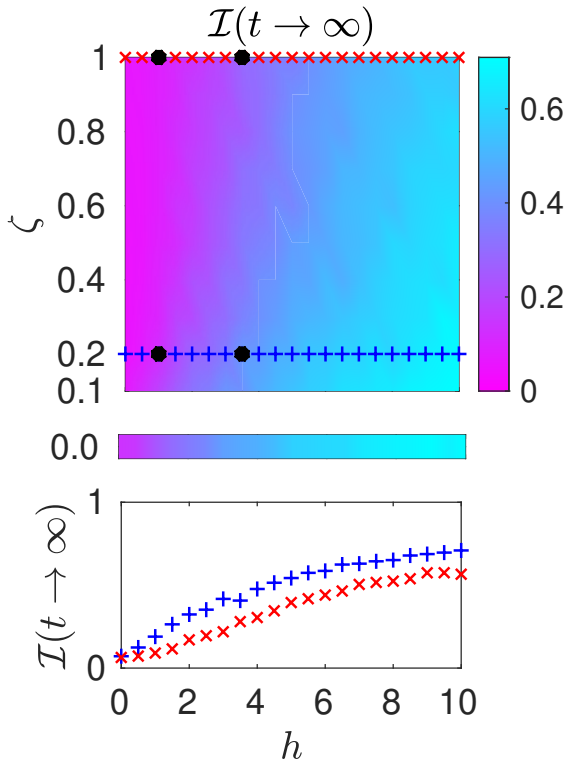

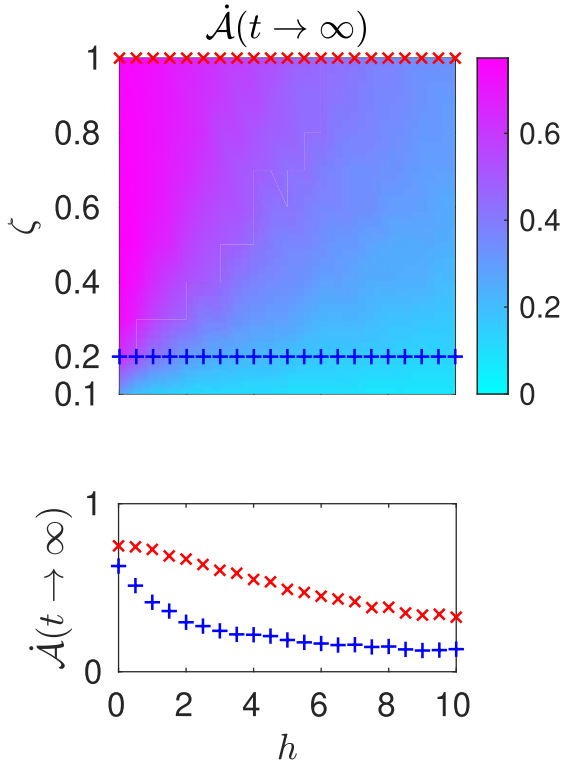

Conclusion: Reducing the number of quantum jumps/Postselection can promote the emergence of the localized phase.

Selective decision making and collective motion of fish via visual attention

Susumu Ito and Nariya Uchida Dept. of Phys., Tohoku Univ.

fish plate agent eye

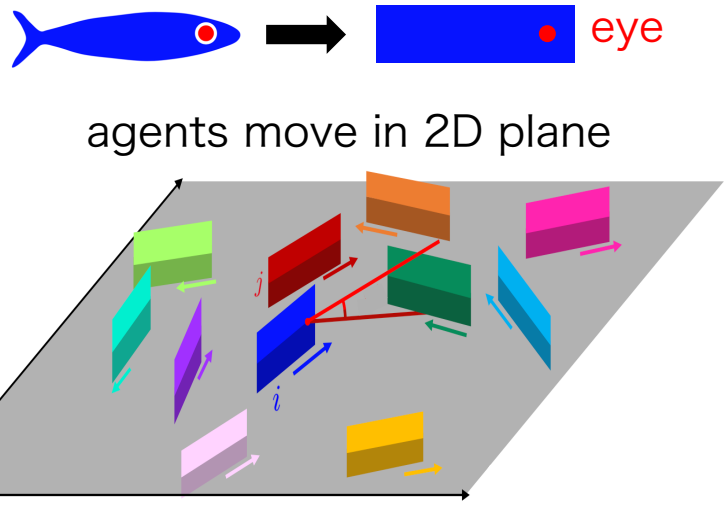

the number of bins corresponds to that of ganglion cells

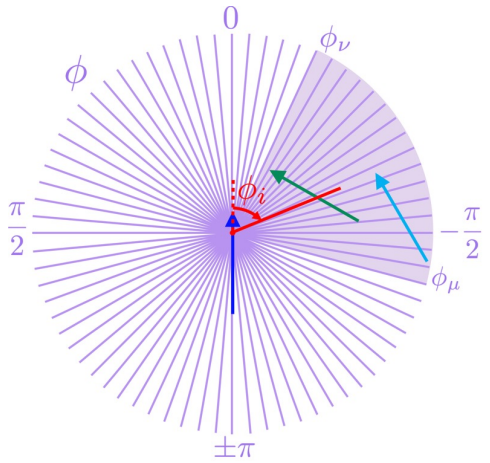

a signal is created on a bin

$\Gamma_i(\phi)$ = sum of signals

angle of visual attention

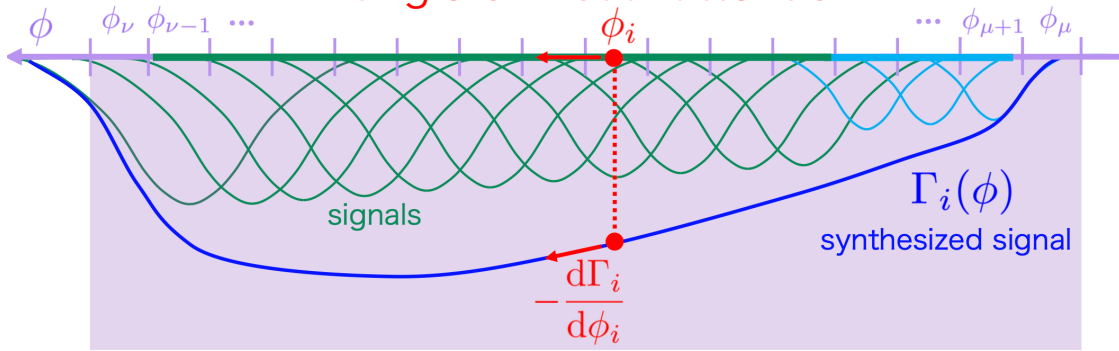

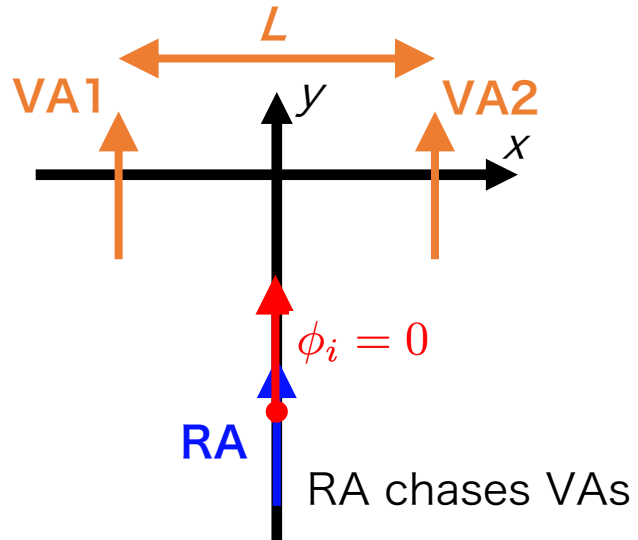

probability distribution for L and x

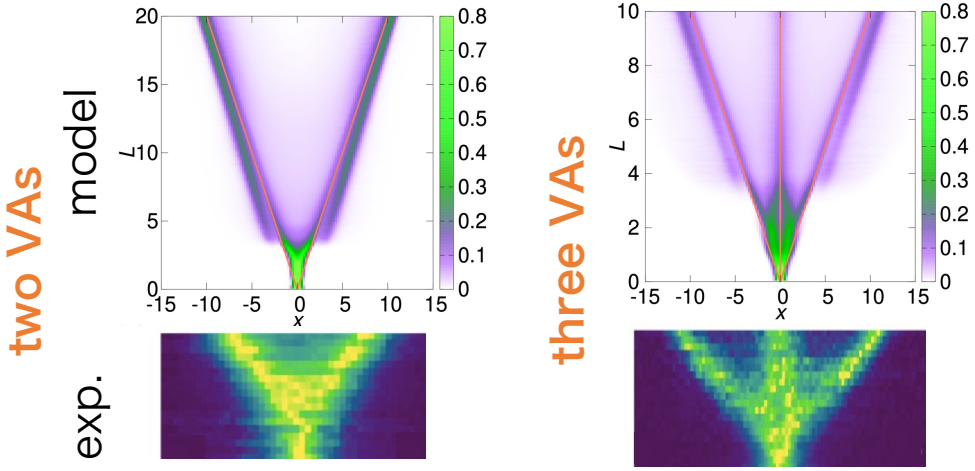

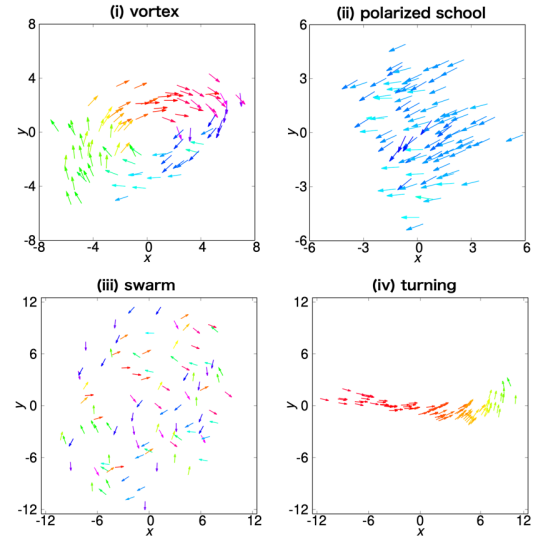

Stability of V-formation of birds by aerodynamic interaction

Hui Jiang, Nariya Uchida

Department of Physics, Tohoku University

Motivation

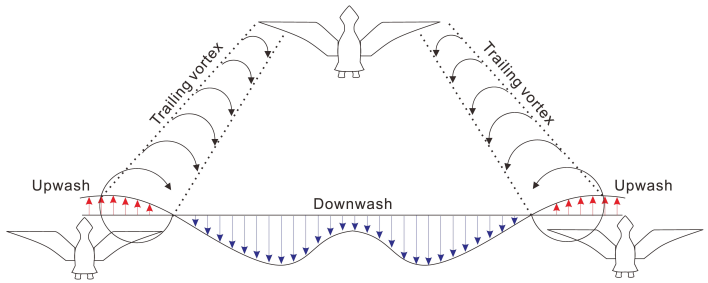

Induced drag:

$$D_I = -2b\rho\Gamma\omega$$

ω:*upwash velocity*

exploit upwash

Model

- **Rectangle model**

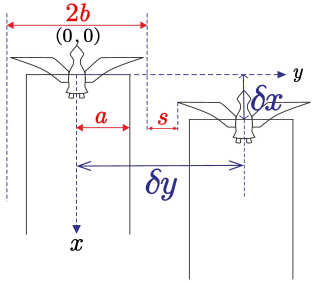

- **Ellipse model**

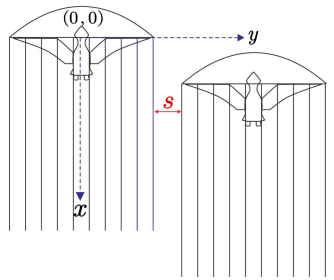

Biot-Savart law

$$\omega(\delta x, \delta y)$$

Result

- **Optimal wingtip spacing**

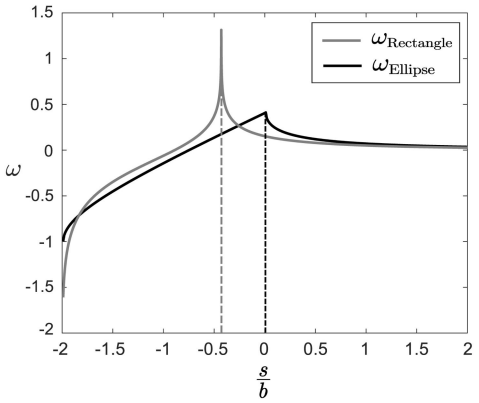

Rectangle: $s_{opt} = (\frac{\pi}{4} - 1)b$

Ellipse: $s_{opt} = 0$

- **θ −dependence (Rectangle model)**

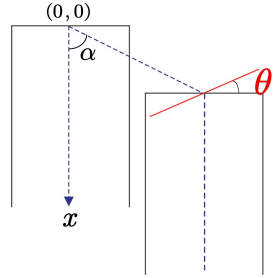

Angular pertubation stable for

$\alpha = \frac{\pi}{4}, \delta x > 2a$ (no crossing vortex)

- **Optimal distance (Ellipse model)**

$$\delta x = 0,\ \delta y = 2b$$

Visual communication necessary for $\delta x > 0$?

Prediction of Tensile Strength, Hardness, and Melting Point of Nickel Superalloys Based on Composition Using Machine Learning

Jaka Fajar Fatriansyah[1], Rio Sudwitama Persadanta Kaban[2]

UNIVERSITAS INDONESIA
Veritas, Probitas, Iustitia
FAKULTAS TEKNIK

Introduction

- Superalloys are a class of materials renowned for retaining mechanical properties at **elevated temperatures**.
- Extreme operating temperature conditions impact the **tensile strength, hardness, and melting point properties**
- Three machine learning models which are **KNN, ANN, and SVR** are used in this study **to predict properties based on composition (C2P)** and **composition based on properties (P2C)**

Targeted Properties

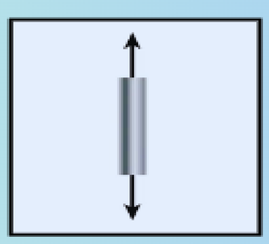

High Tensile Strength

High Hardness

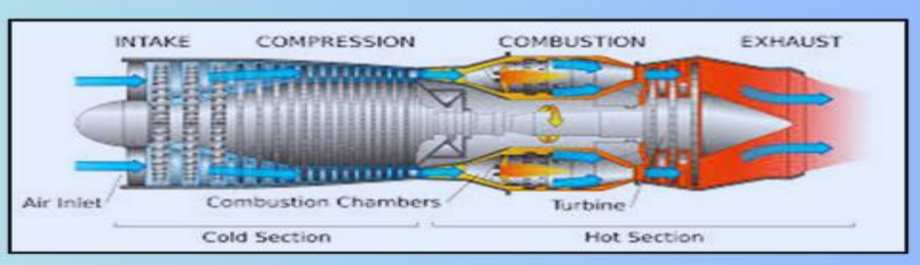

High Melting Point

Research Metodology

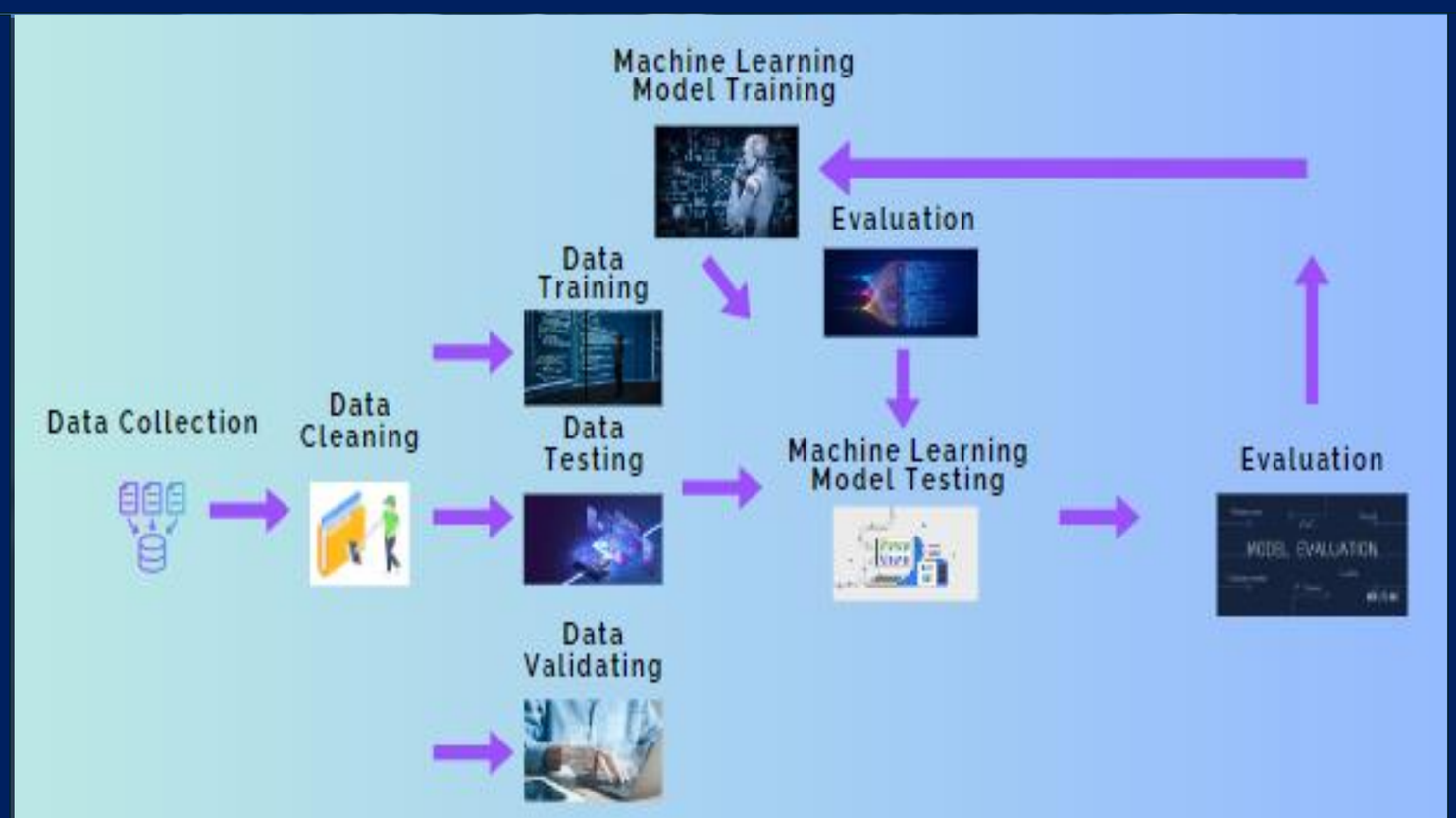

Performance C2P Predictions

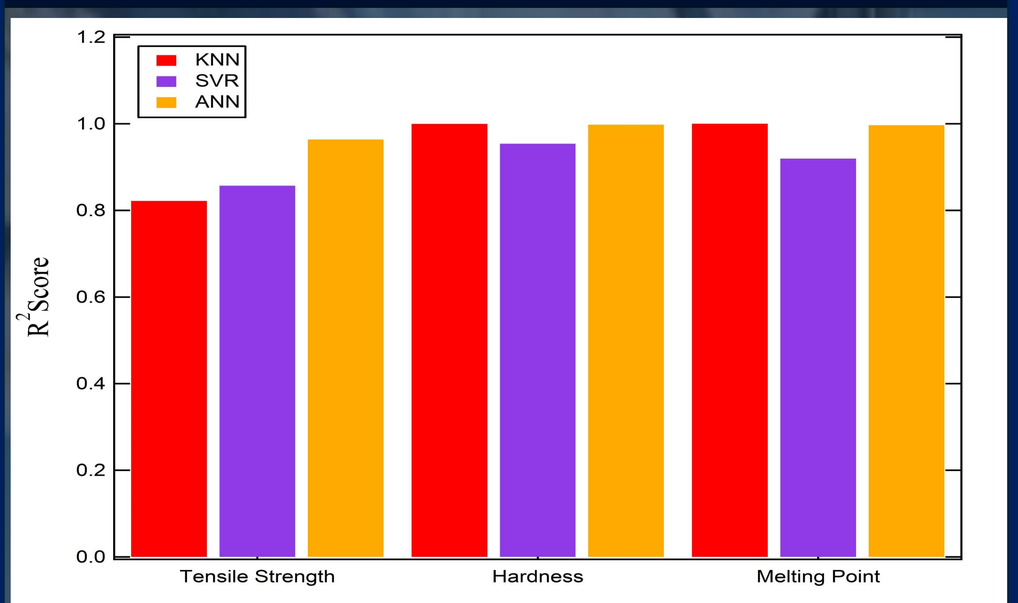

Performance P2C Predictions

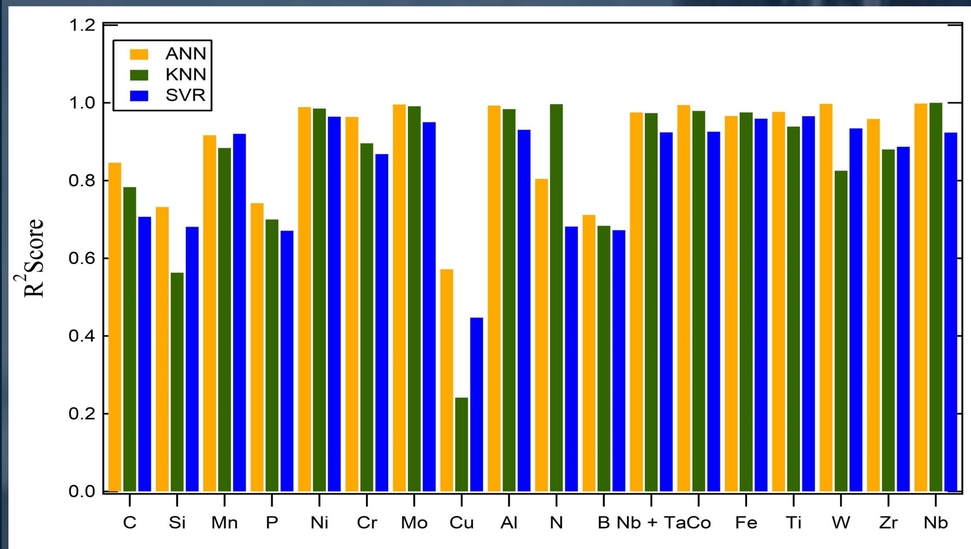

Most Influenced Element for Each Properties

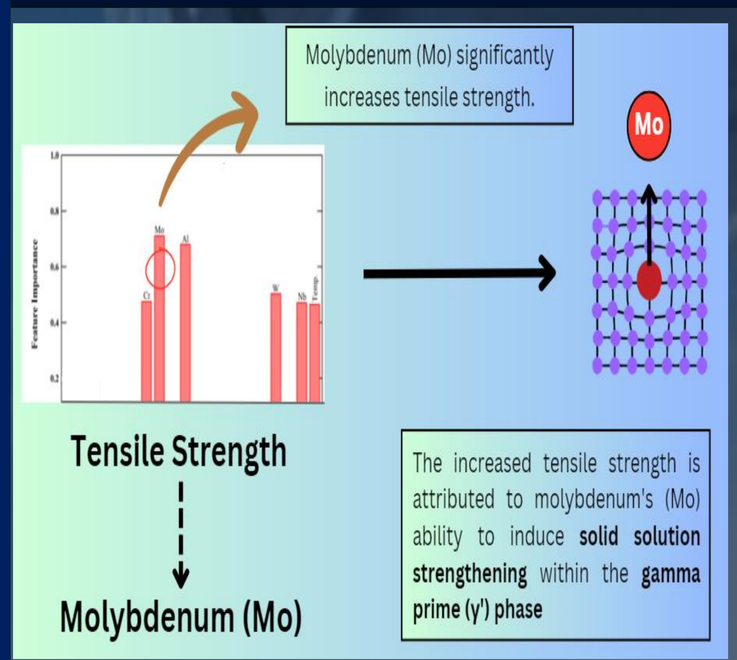

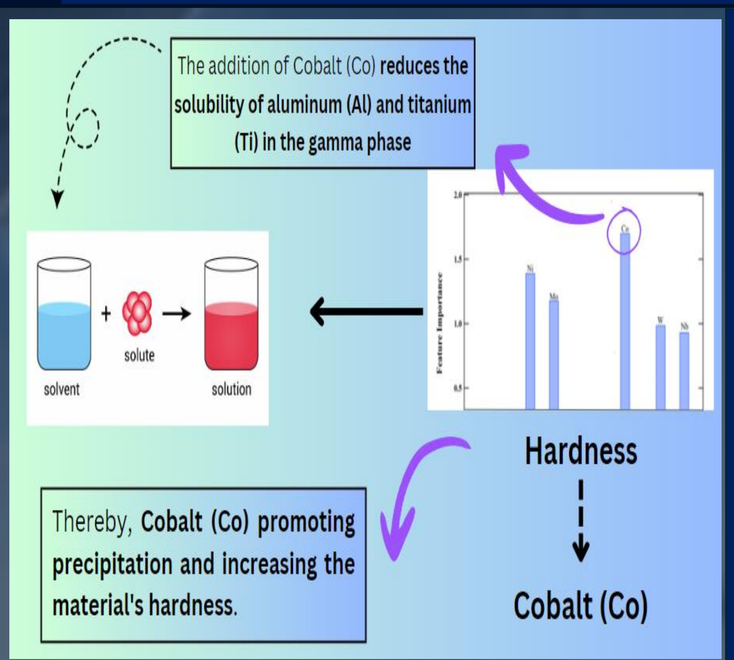

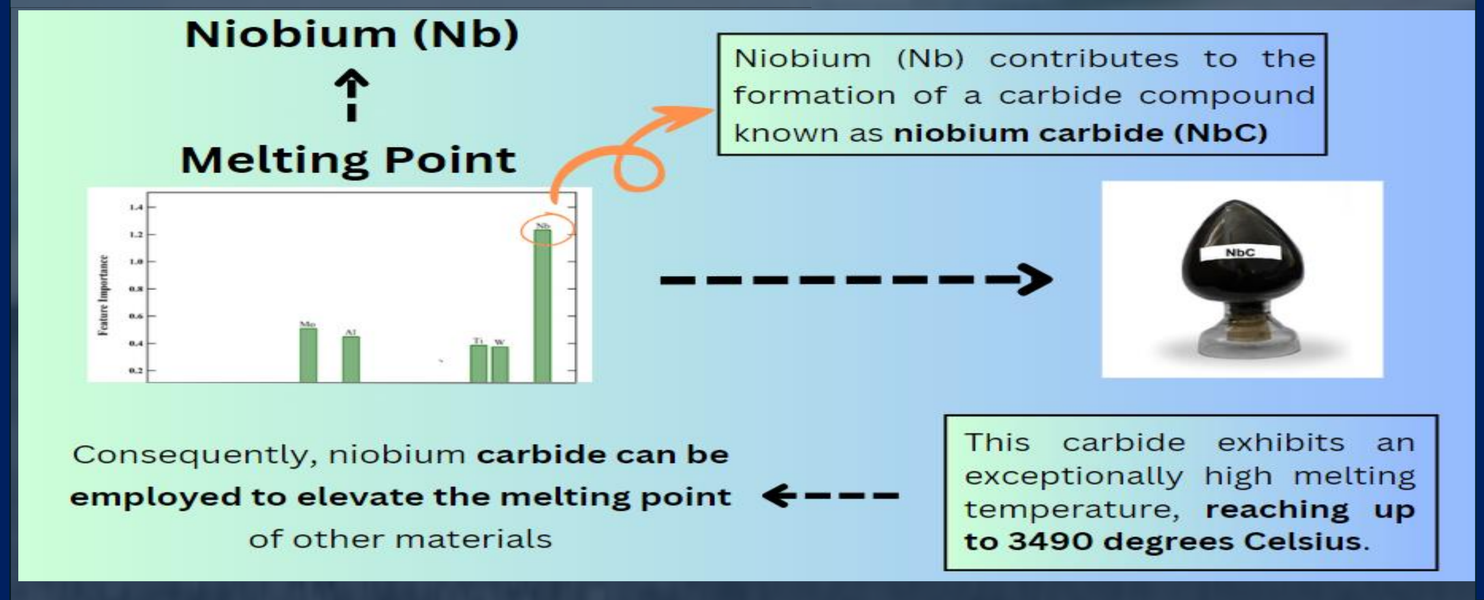

A definition of quantum asymptotic phase function for analyzing quantum synchronization from the Koopman operator viewpoint

Yuzuru Kato, Future University Hakodate

In this poster, we propose a fully quantum-mechanical definition of the asymptotic phase for quantum nonlinear oscillators, a fundamental quantity in the theory of classical nonlinear oscillations.

Synchronization of rhythmic dynamical systems is ubiquitously observed in science and technology, including chemical oscillations, biological rhythms, electrical oscillations, and mechanical vibrations. Recent developments in experimental methodologies have already reached micro- and nano-scales and will soon enter the quantum regime, and the demand for theoretical studies of quantum synchronization is rapidly growing [1]. Several novel features in quantum synchronization have been theoretically analyzed recently, such as multiple-phase locking [2], which are explicit quantum effects arising from the discrete nature of the energy spectrum.

In analyzing synchronization properties of classical nonlinear oscillators, the asymptotic phase of the oscillator is essentially important. It provides the basis for phase reduction, a standard theoretical method for analyzing systems of nonlinear oscillators. It enables us to describe the nonlinear multi-dimensional dynamics of the oscillator by a simple phase equation and has been extensively used to unveil universal synchronization properties of coupled oscillator systems. The collective synchronization transition in a population of coupled oscillators (the Kuramoto model) is the most prominent result predicted by the theory, and the wobbling of the Millennium footbridge in London caused by synchronization of many pedestrians is a well-known real-world example of this universal phenomenon [3].

In our previous study [4], we formulated the phase reduction theory for quantum nonlinear oscillators in the semiclassical regime where the system is represented by a phase-space state fluctuating along a classical trajectory due to small quantum noise. However, this theory is not applicable in the strong quantum regime, because we cannot define the asymptotic phase of the system by using the classical deterministic trajectory. In this study, to overcome this fundamental difficulty, we introduce the asymptotic phase of quantum nonlinear oscillators in a fully quantum-mechanical way, thereby extending its applicability to the strong quantum regime and enabling analysis of nontrivial quantum synchronization phenomena.

We propose a fully quantum-mechanical definition of the asymptotic phase for quantum nonlinear oscillators, a fundamental quantity in the theory of classical nonlinear oscillations. Our definition of the asymptotic phase is based on the eigenoperator of the adjoint Liouville superoperator of the open quantum system. It is inspired by the study on the asymptotic phase of classical stochastic oscillators by Thomas and Lindner [5], which is also natural from the

recently developing Koopman-operator viewpoint on dynamical systems. We analyze a quantum van der Pol oscillator with the Kerr effect and show that our quantum asymptotic phase yields appropriate results in both semiclassical and strong quantum regimes [6, 7].

Quantum synchronization, a burgeoning topic at the boundary between quantum physics and nonlinear physics, is attracting much attention not only in pure and applied physics but also in information science, applied mathematics, and various engineering fields. The quantum asymptotic phase proposed in this study is generally applicable in the strong quantum regime and will serve as a fundamental quantity for characterizing quantum nonlinear oscillators and provide new insights into future applications of quantum synchronization in the evolving field of quantum technologies.

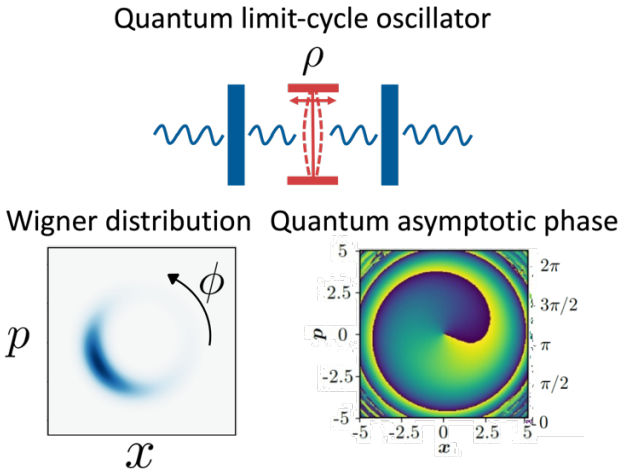

Fig. 1 Quantum limit-cycle oscillators and quantum asymptotic phase

References:

[1] T. E. Lee and H. R. Sadeghpour, "Quantum synchronization of quantum van der Pol oscillators with trapped ions," Phys. Rev. Lett. 111(23), 234101 (2013).

[2] N. Lörch, E. Amitai, A. Nunnenkamp, and C. Bruder, "Genuine quantum signatures in synchronization of anharmonic self-oscillators," Phys. Rev. Lett. 117(7), 073601 (2016).

[3] Y. Kuramoto, Chemical Oscillations, Waves, and Turbulence (Springer, Berlin, 1984).

[4] Y. Kato, N. Yamamoto, and H. Nakao, "Semiclassical phase reduction theory for quantum synchronization," Phys. Rev. Res. 1, 033012 (2019).

[5] P. J. Thomas and B. Lindner, "Asymptotic phase for stochastic oscillators" , Phys. Rev. Lett. 113, 254101 (2014).

[6] Y. Kato and H. Nakao, "A definition of the asymptotic phase for quantum nonlinear oscillators from the Koopman operator viewpoint," Chaos 32, 063133 (2022).

[7] Y. Kato and H. Nakao, "Quantum asymptotic phase reveals signatures of quantum synchronization," New J. Phys. 25 023012 (2023).

Field Disorder and Universality Classes in the Transverse-Field Ising Ferromagnet: A Two-Dimensional Investigation

Heejeong Kim[1], **Seung Ki Baek**[2]

1 Department of Physics, Pukyong National University, Busan, 48513, Korea

2 Department of Scientific Computing, Pukyong National University, Busan, 48513, Korea

2D TFIF with Field Disorder

Hamiltonian

$$H = -J\sum_{\langle ij\rangle}\sigma_i^z\sigma_j^z - \sum_i \Gamma_i\sigma_i^x$$

on the $L \times L$ square lattices

with probability distribution

$$P(\Gamma_i) = \begin{cases} \Gamma_{max}^{-1}, & \text{for } 0 < \Gamma_i < \Gamma_{max} \\ 0, & \text{otherwise} \end{cases}$$

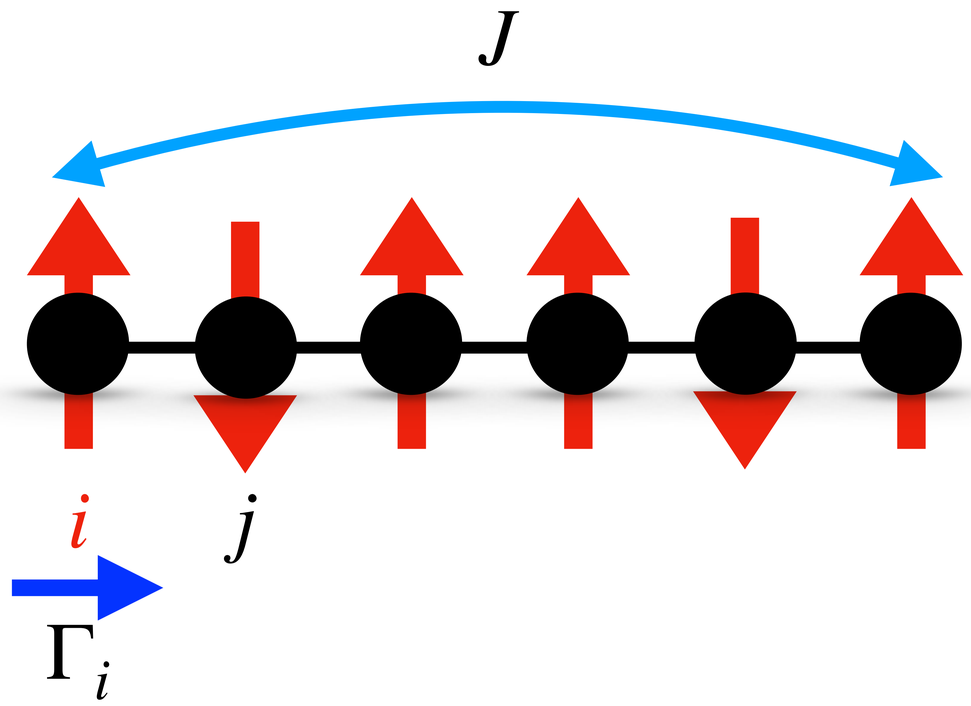

Fig 1. Schematic representation

- Performed quantum Monte-Carlo simulation with path-integral representation in the continuous-time limit.
- We currently estimate critical point, $\Gamma_c \approx 13.7$, and dynamic critical exponent, $z \simeq 2$.

2 min. preview talk

P23 Quantum chaos and Bifurcation in billiard systems

Hironori Makino
Dept. of Human & Info. Sci. at TOKAI Univ.

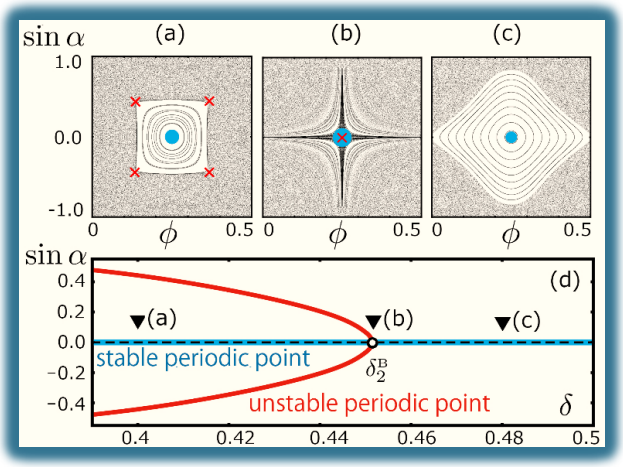

Fig.1 Bifurcation diagram of the Lemon Billiard system.

Is it possible to detect bifurcation points of classical dynamical system from quantum mechanical data?

→ Yes, it is!

They can be detected by analysing the energy levels and energy eigenfunction of the corresponding quantum system.

- The energy levels at the bifurcation points show a strong accumulation on the energy axis with a certain period P_2, and this period is well predicted by the Gutzwiller's semiclassical theory (see Fig.2).

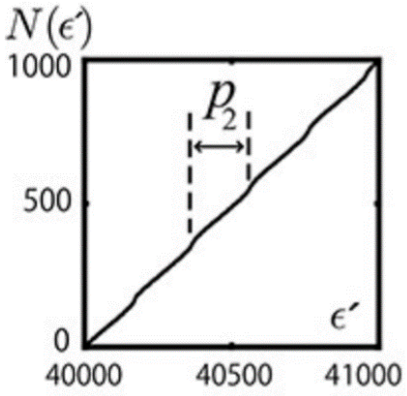

Fig.2 Integrated density of states. P_2 is the accumulation period.

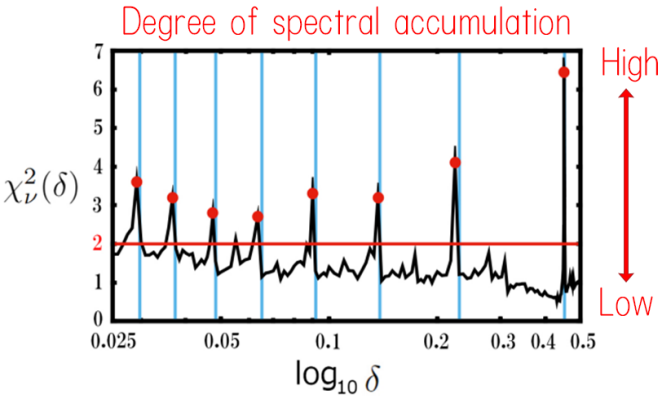

Fig.3 Degree of energy level accumulation χ^2 vs the bifurcation parameters δ (Blue lines). Is's quantum mechanical predictions are plotted by the red marks●.

- By observing this accumulation quantitatively, we can obtain predicted values of the bifurcation parameters (red marks ● in Fig. 3), which are in good agreement with the bifurcation points of the classical dynamical system (blue lines in Fig. 3).

2 min. preview talk

We also analyse the energy eigenfunctions at the bifurcation points of Fig.3(at the red marks), and observed the eigenfunction scarring.

- The energy eigenfunctions at each accumulation point are strongly amplified along the bifurcating orbits (Fig.4), and always be the eigenfunction scarring. T This phenomenon also occurs periodically along the energy axis with the period P_2 (see Fig.5).
- By observing this phenomenon quantitatively, we attempt to estimate the position of a fixed point on the Poincaré surface of section.

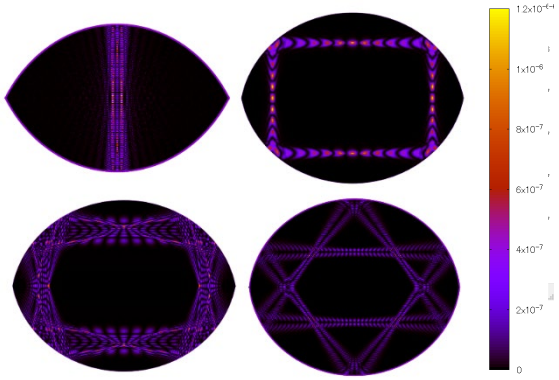

Fig.4 Typical eigenfunction scarrings at the bifurcation points, strongly amplified along the bifurcating orbits.

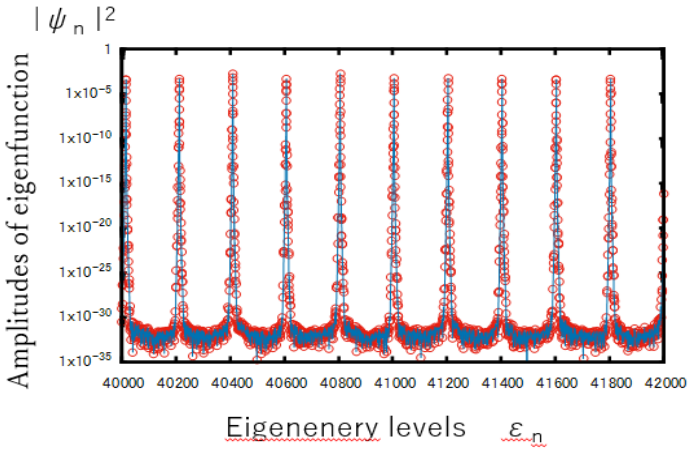

Fig.5 Amplitudes $|\psi_n|^2$ of energy eigenfunctions on bifurcated orbits.

Summary

I. By observing the accumulation of quantal energy levels, one can predict the bifurcation parameters of classical dynamical system.

II. The eigenfunction scarring is induced frequently at the bifurcation points and it is associated with the periodic accumulation of quantal levels. However, it's mechanism is not obvious.

Stochastic fluctuating model for two cilia synchronization

Qin Jing, Department of Physics, Tohoku University

Energy dissipation in a noise synchronizing system?
in the weak coupling & weak noise approximation

Model:

$$\begin{aligned}\frac{d\phi_1}{dt} &= \omega_t + K\omega\sin(\phi_2-\delta)\sin\phi_1 + \sqrt{2D}\sqrt{\omega}\xi_1 \\ \frac{d\phi_2}{dt} &= \omega_t + K\omega\sin(\phi_1-\delta)\sin\phi_2 + \sqrt{2D}\sqrt{\omega}\xi_2\end{aligned}$$

Results:

- The synchronized state maximizes the heat dissipation related to the detail of trajectory.
- Computed the heat release specifically on the first order approximation and found it's time-dependence.

Boltzmann-Ginzburg-Landau theory for active particles with chemotaxis and orientational interaction

Shun Sakurai and Nariya Uchida
(Dept. of Phys., Tohoku Univ.)

Self-propelled rods + chemotaxis

$$\theta_j^{t+\Delta t} = \arg \sum_{|r_j - r_k| < d_0} \underbrace{\mathrm{sign}[\cos(\theta_k^t - \theta_j^t)]\exp(i\theta_k^t)}_{\text{nematic interaction}} + \boxed{\zeta_{rot}\partial_\theta \mathbf{e}(\theta_j^t)\cdot\nabla c(\mathbf{r}_j^t)\Delta t}_{\text{rotational chemotaxis}} + \eta_j^t$$

$$\mathbf{r}_j^{t+\Delta t} = \mathbf{r}_j^t + v_0 \Delta t \mathbf{e}(\theta_j^{t+\Delta t}) + \boxed{\zeta_{tr}\nabla c(\mathbf{r}_j^t)\Delta t}$$

translational chemotaxis

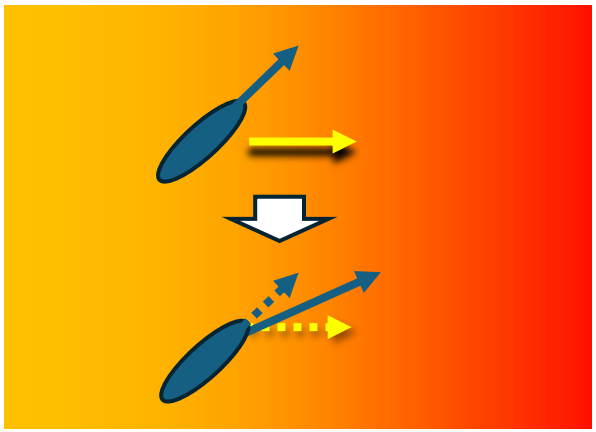

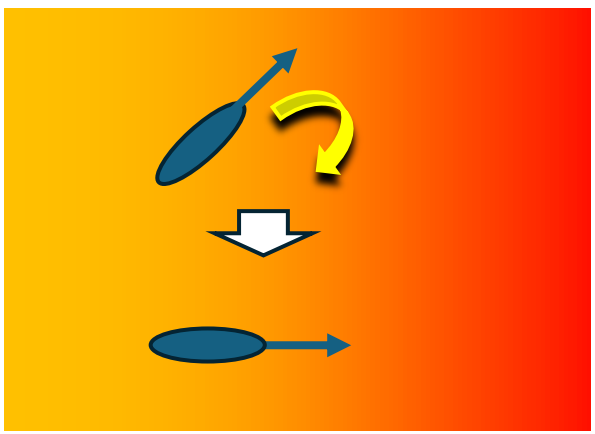

∇c

attractant gradient

Boltzmann equation

With the assumption it is **dilute**, derive the Boltzmann equation of the probability distribution $f(\mathbf{r}, \theta, t)$

$$\partial_t f(r,\theta,t) + v_0 e(\theta)\cdot\nabla f(r,\theta,t) = I_{dif}[f] + I_{col}[f] + D_0\Delta f(r,\theta,t) + D_1 Q_{\alpha\beta}\partial_\alpha\partial_\beta f(r,\theta,t) + \zeta_{rot}\partial_\theta(\partial_\theta e\cdot f\nabla c) - \zeta_{tr}\nabla\cdot(f\nabla c)$$

Linear stability analysis

Instability region of the uniform steady state

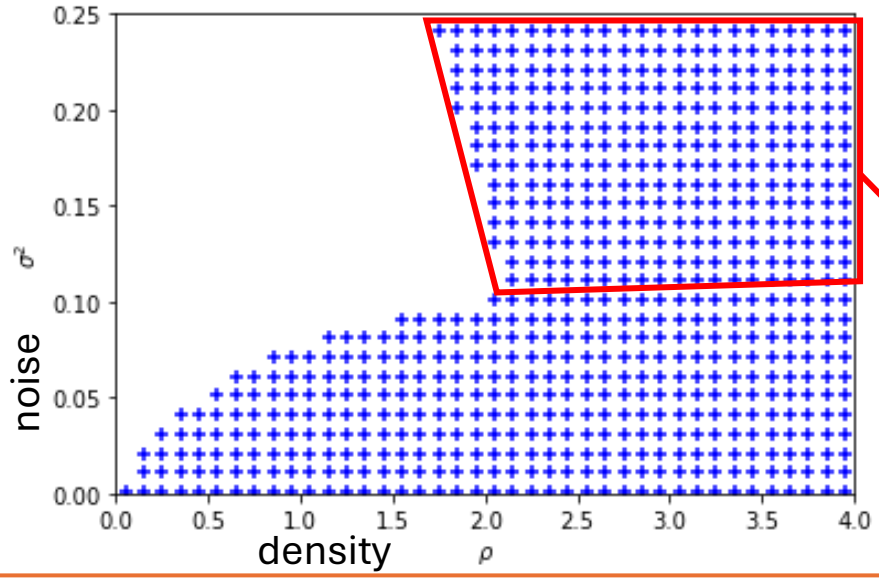

Perform linear stability analysis of the uniform steady solutions of the Boltzmann equation

We obtained the additional instability region caused by chemotaxis.

Optimal figure of merit of low-dissipation quantum refrigerators

Jingyi Chen, Youlin Wang, Jincan Chen, and Shanhe Su
Department of Physics, Xiamen University
* sushanhe@xmu.edu.cn

Abstract

We establish a finite-time external field-driven quantum tricycle model. Within the framework of slow driving perturbation, the perturbation expansion of heat in powers of time can be derived during the heat exchange processes. Employing the method of Lagrange multiplier, we optimize the cooling performance of the tricycle by considering the cooling rate and the figure of merit, which is the product of the coefficient of performance and cooling rate, as objective functions. Our findings reveal the optimal operating region of the tricycle, shedding light on its efficient performance.

1. The control protocol of a finite-time quantum tricycle

The working substance is a two level system (TLS) with time-dependent Hamiltonian $H(t)=\hbar\omega_v(t)\sigma_z/2$, where $\omega_v(t)$ is the energy splitting at time t. A weak coupling between the system and reservoir is considered. The density operator $\rho(t)$ of the TLS evolves according to the Markovian master equation, i,e.,

$$d\rho(t)/dt=\mathcal{L}_v(t)\left[\rho(t)\right],$$

where the generator $\mathcal{L}_v(t)$ represents the quantum Liouvillian superoperator. By introducing the dimensionless time-rescaled parameter $s=t/\tau_v$, the equation can be rewritten as[1]

$$\tilde{\rho}(s)=\tilde{\rho}_{\mathrm{eq},v}(s)+\frac{1}{\tau_v}\tilde{\mathcal{L}}_v^{-1}(s)\frac{d}{ds}\left[\tilde{\rho}_{\mathrm{eq},v}(s)\right],$$

where $\tilde{\mathcal{L}}_v^{-1}(s)$ is the Drazin inverse of $\tilde{\mathcal{L}}_v(s)$. By applying Alicki's definition of heat and the first order perturbation, the amount of heat entering the system from bath during the interval would be

$$Q_v=Q_v^0+Q_v^1=\beta_v^{-1}\left(\Delta S_{\mathrm{eq},v}+\Sigma_v/\tau_v\right),$$

where the first order irreversible corrections of heat can be written by

$$\Sigma_v=\beta_v\int_0^1 ds\,\mathrm{Tr}\left[\tilde{H}(s)\frac{d}{ds}\left\{\tilde{\mathcal{L}}_v^{-1}(s)\frac{d}{ds}\left[\tilde{\rho}_{\mathrm{eq},v}(s)\right]\right\}\right].$$

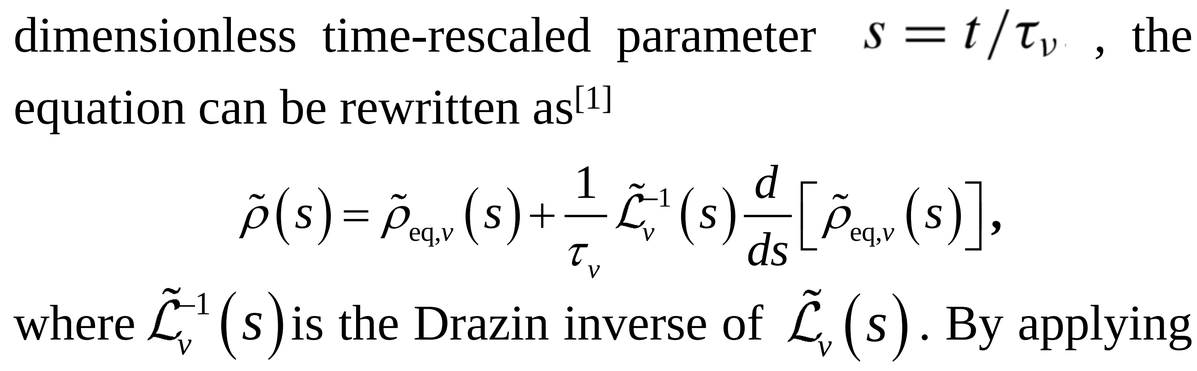

Fig.1. (a) Schematic representation of a quantum tricycle. (b) The temperature-entropy diagram of a FTQTC. (c) The temperature-entropy diagram of a reversible quantum tricycle.

The detail of the control protocols of the quantum tricycle are designed as follows:

A→B: Heat exchange with reservoir c

$$\omega_c(t)=\delta_c\left[\cos\pi\left(t/\tau_c\right)+\zeta_c\right]$$

B→C: Diabatic expansion

$$\omega_c(\tau_c)\to\omega_h(0)=\left(T_h/T_c\right)\omega_c(\tau_c)$$

C→D: Heat exchange with reservoir h

$$\omega_h(t)=\delta_h[\cos(\pi t/\tau_h)+\zeta_h]$$

D→E: First diabatic expansion p

$$\omega_h(\tau_h)\to\omega_p(0)=\left(T_p/T_h\right)\omega_h(\tau_h)$$

E→F: Heat exchange with reservoir

$$\omega_p(t)=\delta_p[\cos(\pi(1-t)/\tau_p)+\zeta_p]$$

F →A: Second diabatic expansion

$$\omega_p(\tau_p)\to\omega_c(0)=\left(T_c/T_p\right)\omega_p(\tau_p)$$

2. The relationships between the amplitude and the displacement

$$\omega_c(\tau_c)=\left(T_c/T_h\right)\omega_h(0)$$
$$\omega_h(\tau_h)=\left(T_h/T_p\right)\omega_p(0)$$
$$\omega_p(\tau_p)=\left(T_p/T_c\right)\omega_c(0)$$

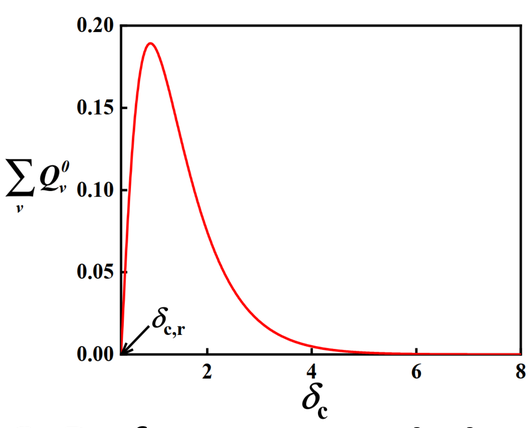

$$\frac{\delta_c(\zeta_c-1)}{\delta_h(\zeta_h+1)}=\frac{T_c}{T_h},\quad \zeta_p=\frac{1+\zeta_c\zeta_h}{\zeta_c+\zeta_h},$$
$$\frac{\delta_h(\zeta_h-1)}{\delta_p(\zeta_p-1)}=\frac{T_h}{T_p},\quad \delta_h=\frac{T_h(\zeta_c-1)}{T_c(1+\zeta_h)}\delta_c,$$
$$\frac{\delta_p(\zeta_p+1)}{\delta_c(\zeta_c+1)}=\frac{T_p}{T_c}.\quad \delta_p=\frac{T_p(\zeta_c+\zeta_h)}{T_c(1+\zeta_h)}\delta_c.$$

Fig.2. The curves of the sum of the zeroth order approximation of heat varying with the amplitude frequency.

3. Performance optimization in the slow-driving regime

We can generate the optimal curve of the cooling rate varying with the COP for given frequency exponent α. The frequency α exponent determines the spectral density

$$J(\omega_v(t))\propto[\omega_v(t)]^\alpha$$

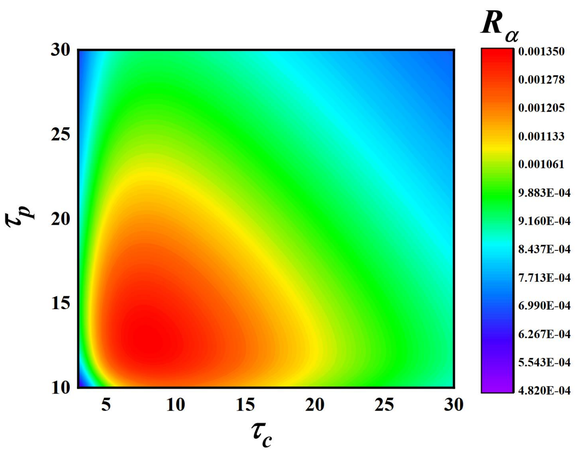

Fig.3. Plot of the cooling rate R with respect to time τ_c and τ_p.

4. Result

$$R=\frac{Q_c}{\tau_c+\tau_h+\tau_p}=\frac{T_c\left[\Delta S_{eq,c}+\Sigma_c/\tau_c\right]}{\tau_c+\tau_h+\tau_p}.$$

$$\psi=\frac{Q_c}{Q_h}=\frac{T_c\left[\Delta S_{eq,c}+\Sigma_c/\tau_c\right]}{T_h\left[\Delta S_{eq,h}+\Sigma_h/\tau_h\right]},$$

$$L(\tau_c,\tau_h,\tau_p)=R+\lambda_1\psi+\lambda_2\left(Q_c+Q_h+Q_p\right),$$

$$\Delta S_{eq,h}\frac{\tau_h^2}{\Sigma_h}+\Delta S_{eq,p}\frac{\tau_p^2}{\Sigma_p}+\Delta S_{eq,c}\frac{\tau_c^2}{\Sigma_c}+2\left(\tau_c+\tau_h+\tau_p\right)=0.$$

$$\tau_h=-\frac{T_h\Sigma_h}{T_p\left(\Delta S_{eq,p}+\Sigma_p/\tau_p\right)+T_c\left(\Delta S_{eq,c}+\Sigma_c/\tau_c\right)+T_h\Delta S_{eq,h}}.$$

The figure of merit $\chi=\psi R$ can be commonly employed as a target function for optimizing the performance of refrigerators

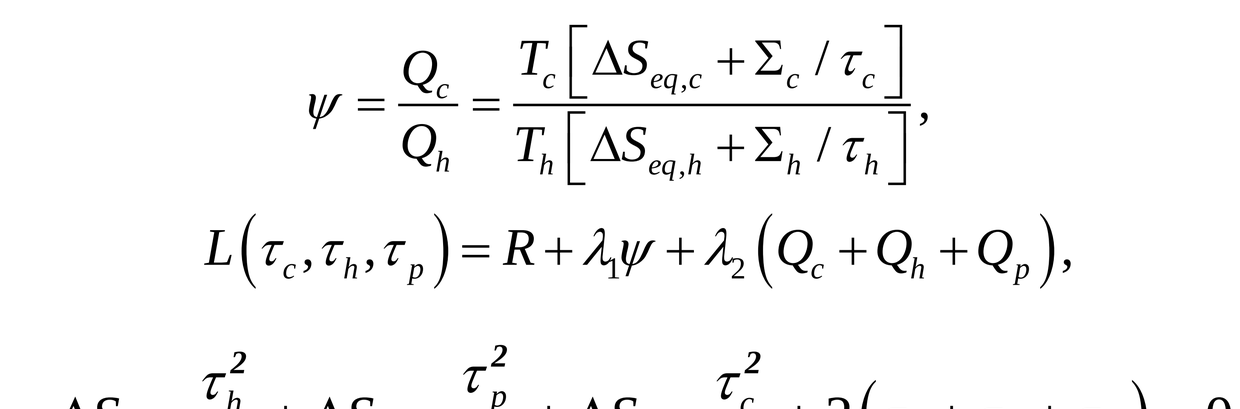

Fig.4. (a) Plot of the cooling rate and figure of merit varying with the COP. (b) Plot of the cooling rate and figure of merit varying with the α. (c) The optimum characteristic curves of the cooling rate and the figure of merit varying with COP .

References: [1] V. Cavina, A. Mari, and V. Giovannetti, Phys. Rev. Lett. 119, 050601 (2017).
[2] J. Y. Chen, S. H. Xia, J. C. Chen, and S. H. Su, Performance optimization of the finite-time quantum tricycle[J]. (Under review)

Acknowledgments: The National Natural Science Foundation of China (Grant No. 11805159 and 12075197)

Bifurcation analysis of spatiotemporal dynamics in the one-dimensional non-reciprocal Swift-Hohenberg model (P37.)

Yuta Tateyama[1], Hiroaki Ito[1], Shigeyuki Komura[2], and Hiroyuki Kitahata[1] ([1]Chiba Univ., [2]WIUCAS)

Non-reciprocal interaction system

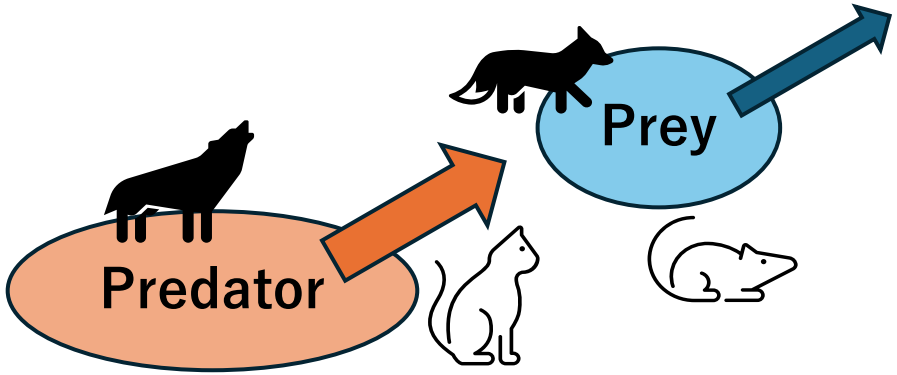

Non-reciprocal Swift-Hohenberg (NRSH) model

$$\begin{cases} \partial_t \phi = \left[\varepsilon - \left(1+\partial_x^2\right)^2\right]\phi - \phi^3 - (\chi + \alpha)\psi \\ \partial_t \psi = \left[\varepsilon - \left(1+\partial_x^2\right)^2\right]\psi - \psi^3 - (\chi - \alpha)\phi \end{cases}$$

inhibition (+α) / activation (−α)

Swift-Hohenberg equation + non-reciprocity

"Spurious" gradient dynamics

$$\begin{cases} \partial_t \phi = -\dfrac{\delta F}{\delta \phi} - \alpha \dfrac{\delta F^{\mathrm{NR}}}{\delta \phi} \\ \partial_t \psi = -\dfrac{\delta F}{\delta \psi} + \alpha \dfrac{\delta F^{\mathrm{NR}}}{\delta \psi} \end{cases}$$

inhibition (−α) / activation (+α)

gradient dynamics + non-reciprocity

Spatiotemporal patterns of 1D NRSH model

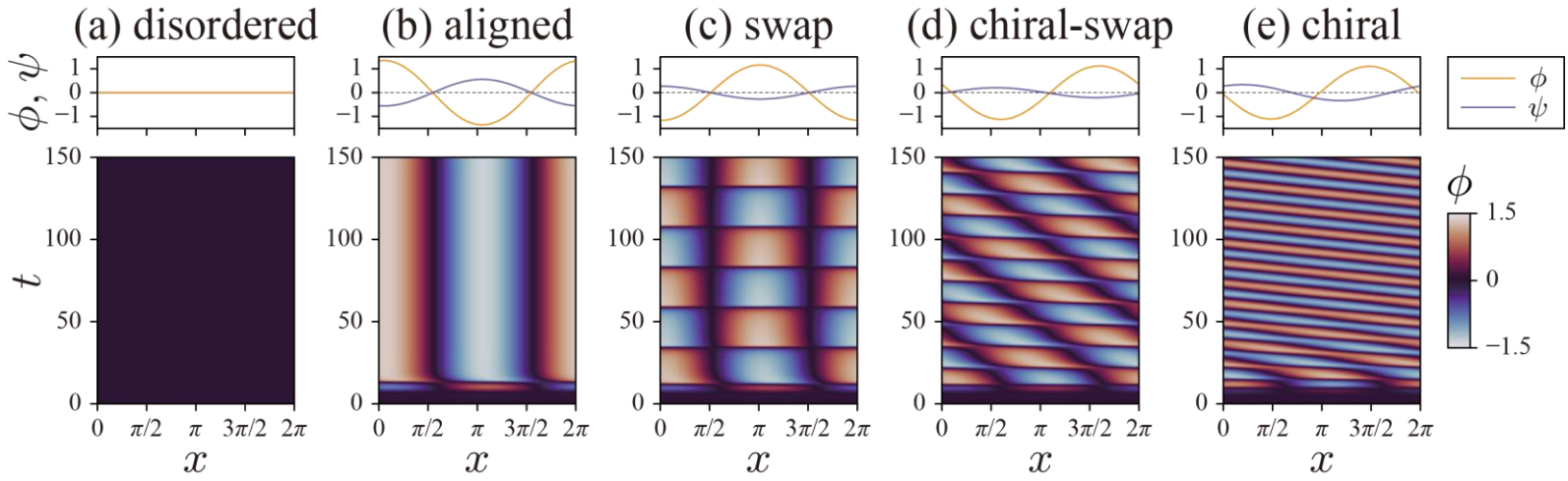

M. Fruchart *et al.*, *Nature*, 2021.

Bifurcation analysis of spatiotemporal dynamics in the one-dimensional non-reciprocal Swift-Hohenberg model (P37.)

Yuta Tateyama[1], Hiroaki Ito[1], Shigeyuki Komura[2], and Hiroyuki Kitahata[1] ([1]Chiba Univ., [2]WIUCAS)

Reduced ODE system for spatial Fourier mode

$$\begin{cases} \dot{\rho}_1 = \varepsilon\rho_1 - 3\rho_1^3 - (\chi+\alpha)\rho_2\cos\delta \\ \dot{\rho}_2 = \varepsilon\rho_2 - 3\rho_2^3 - (\chi-\alpha)\rho_1\cos\delta \\ \dot{\delta} = \left[(\chi-\alpha)\dfrac{\rho_1}{\rho_2} + (\chi+\alpha)\dfrac{\rho_2}{\rho_1}\right]\sin\delta \end{cases}$$

Connection of branches for the reduced ODE

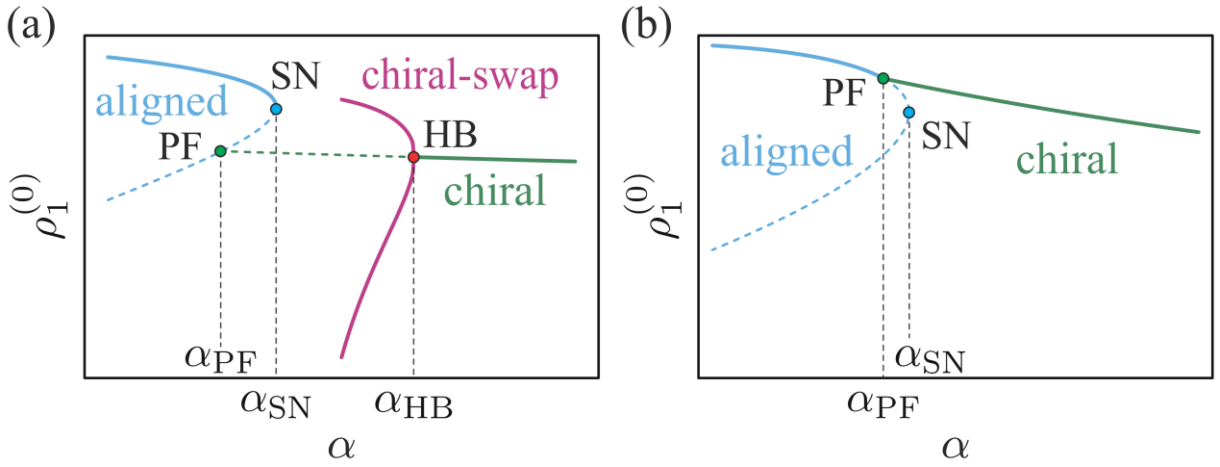

Phase diagram of the 1D NRSH model

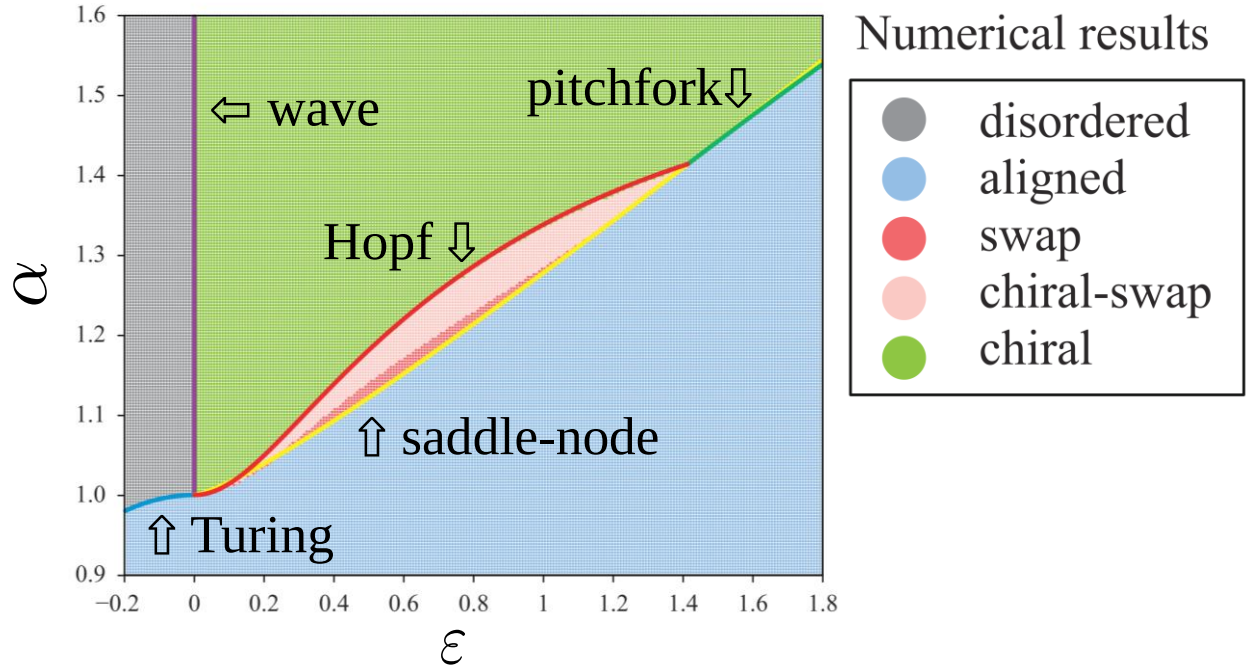

Bifurcation analysis of the reduced ODE system explains the spatiotemporal patterns of the 1D NRSH model.

#39: Tracking Chemical Reaction Networks Driven Time-Periodically from the Viewpoint of Condensed Matter Physics

Yuki Watanabe[A], Zoé Jeandupeux[B], Yuki Ishiguro[C,D], Masafumi Udagawa[E], Shintaro Takayoshi[F], Takashi Oka[D]
Univ. Tokyo[A], EPFL[B], Tokyo Polytech[C], ISSP[D], Gakushuin Univ.[E], Konan Univ.[F]

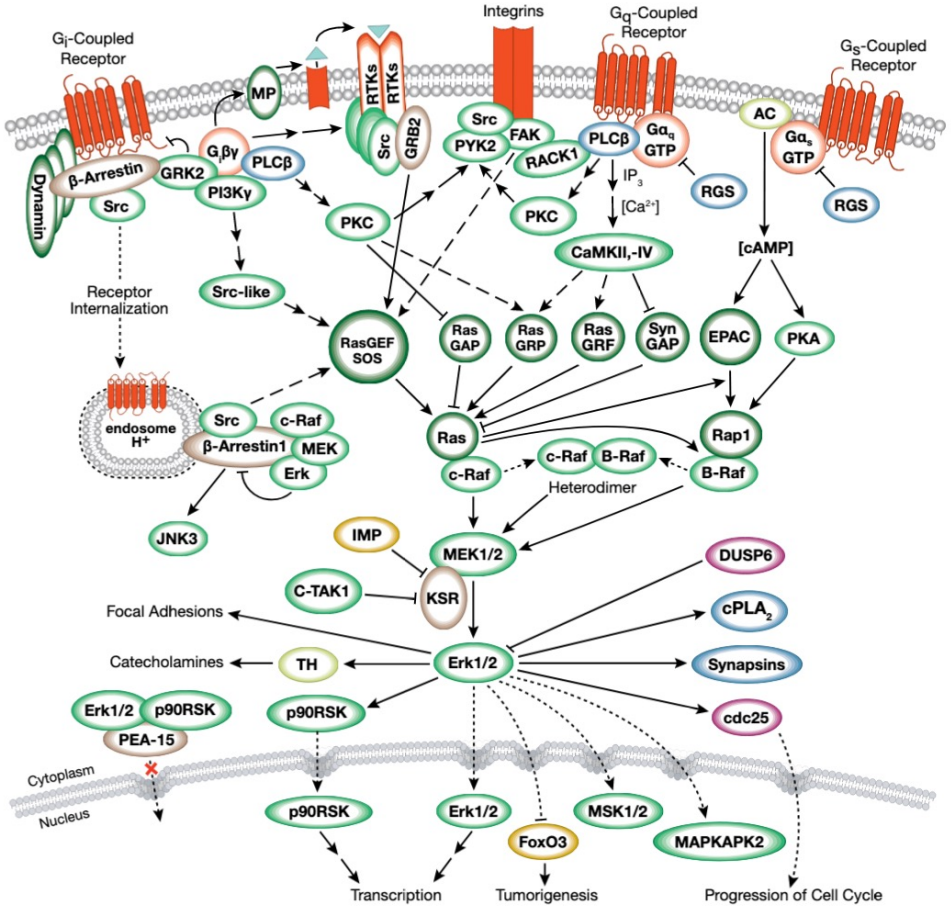

Example of a chemical reaction network (Signaling from G protein-coupled receptors to MAPK/Erk) 2023 © Cell Signaling Technology.

Master equation

$$\frac{\mathrm{d}}{\mathrm{d}t}P(\alpha,t)=\sum_{\beta}\left[W(\alpha|\beta)P(\beta,t)-W(\beta|\alpha)P(\alpha,t)\right]$$

2nd quantization

M. Doi, J. Phys. A: Math. Gen. **9**, 1465 (1976).
L. Peliti, J. Phys. France. **46**, 1469-83 (1985).

Schrödinger equation (imaginary time) of open quantum system

$$\frac{\mathrm{d}}{\mathrm{d}t}\left|\psi(t)\right\rangle=-\hat{H}\left|\psi(t)\right\rangle,\quad \left|\psi(t)\right\rangle=\sum_{\alpha}P(\alpha,t)\left|\alpha\right\rangle,$$
$$\hat{H}=\hat{H}_{\mathrm{reaction}}+\hat{H}_{\mathrm{diffusion}}$$

S. B. Nicholson and T. R. Gingrich (2023)

Chemical Reaction Network
= Open Quantum System

#39: Tracking Chemical Reaction Networks Driven Time-Periodically from the Viewpoint of Condensed Matter Physics

Yuki Watanabe[A], Zoé Jeandupeux[B], Yuki Ishiguro[C,D], Masafumi Udagawa[E], Shintaro Takayoshi[F], Takashi Oka[D]
Univ. Tokyo[A], EPFL[B], Tokyo Polytech[C], ISSP[D], Gakushuin Univ.[E], Konan Univ.[F]

Chemical Reaction Network
= Open Quantum System (OQS)

Can the state within a living organism be controlled?

II

Can the sate of OQS be controlled?

→ Floquet Engineering of OQS

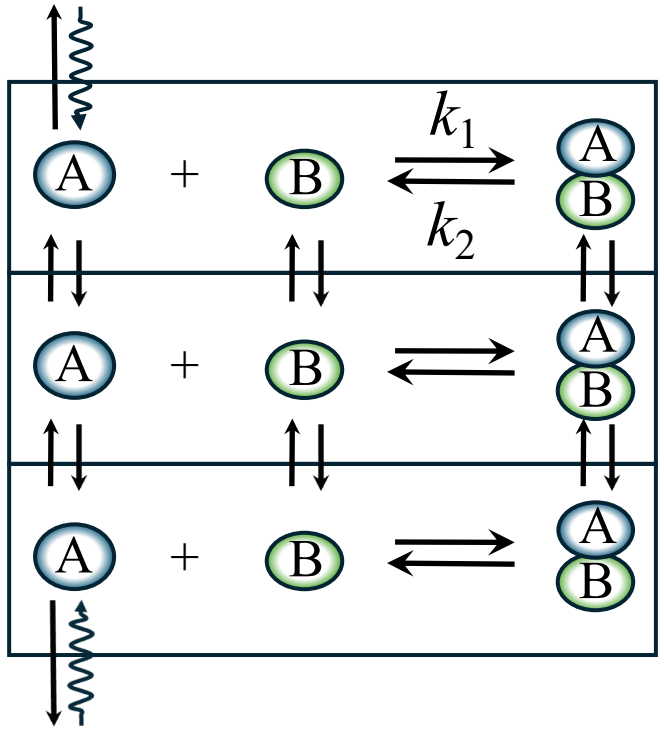

The Result for simple association-dissociation reaction + diffusion

Decoherence in quantum active particles: towards classical active particles?

Keyword:
*Non-equilibrium
*Quantum walk
*Active matter

Manami Yamagishi [1] , Naomichi Hatano [2] , Hideaki Obuse [2, 3]
[1] Dept. of Phys. and [2] IIS, U Tokyo, [3] Dept. of Appl. Phys., Hokkaido U

? How to define active matter (well studied in classical systems) in a quantum system?

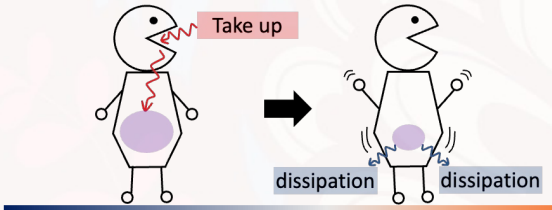

Our "Quantum active matter"
1. System without energy nor momentum conservation
2. Particle moves depending on its internal state

! In a quantum system,
✓ Obtain similar results with a previous research in a classical system
✓ Observe unique features

New research field

Systems w/o energy conservation

	Momentum conserved	Momentum not conserved
Classical	Dissipative system	Active matter
Quantum	Non-Hermitian physics	**Quantum active matter**

Previous research

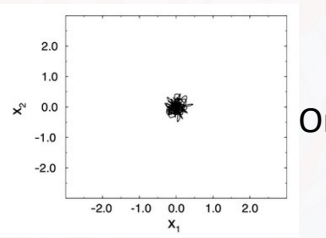

Ordinary

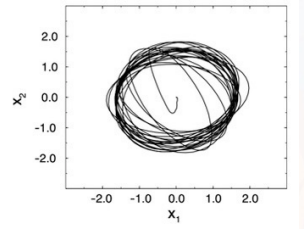

Active

F. Schweitzer *et al.*, PRL. **80**, 5044-5047 (1998).

- M. Yamagishi, N. Hatano and H. Obuse, arXiv:2305.15319 (2023).

➢Using non-unitary quantum walks…

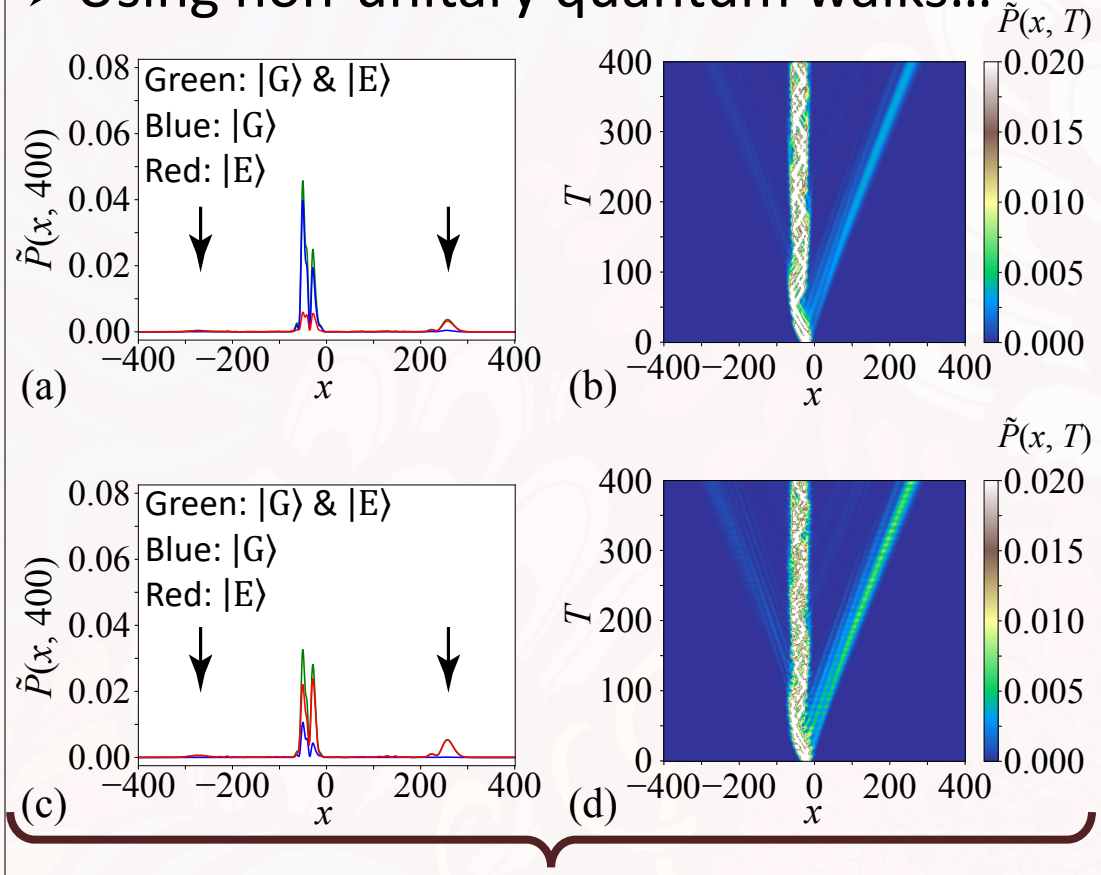

Under effective harmonic potential

(a)&(b): Ordinary ($g = 0$),
(c)&(d): Active ($g = 1$)

🤔 Classical limit?

➢Numerically introduce decoherence in the form of

$$\rho^{\text{new}} = (1-p)U\rho U^{\dagger} + p\,\text{diag}\left(U\rho U^{\dagger}\right)$$

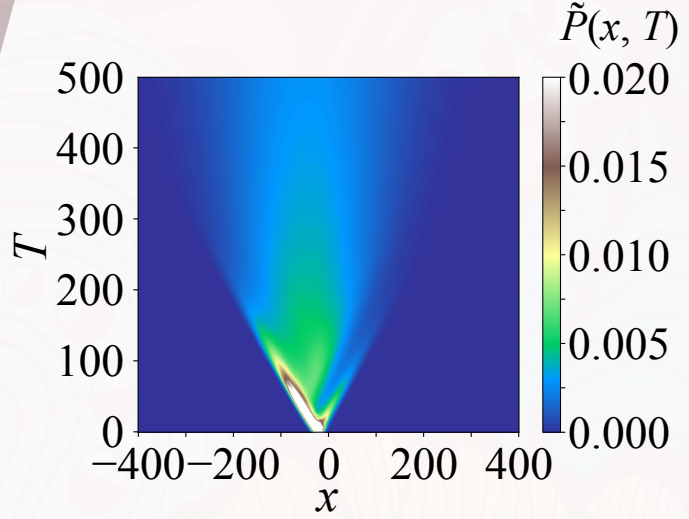

$p = 0.1$
$g = 1$

Discontinuous codimension-two bifurcation in a Vlasov system

Y. Y. Yamaguchi (Kyoto Univ) & J. Barré (Univ Orléans)

What is the Vlasov (collisionless Boltzmann) system?

= Dynamics of long-range Hamiltonian system by 1-body dist

Examples:

- Self-gravitating systems
- Plasmas
- 2D Euler fluids
- Ising/XY spins

Bifurcation in Vlasov: Assume the position q is periodic

1-body dist $F_{\rm ini}(\cancel{q}, p)$: Non-clusterd state is stationary

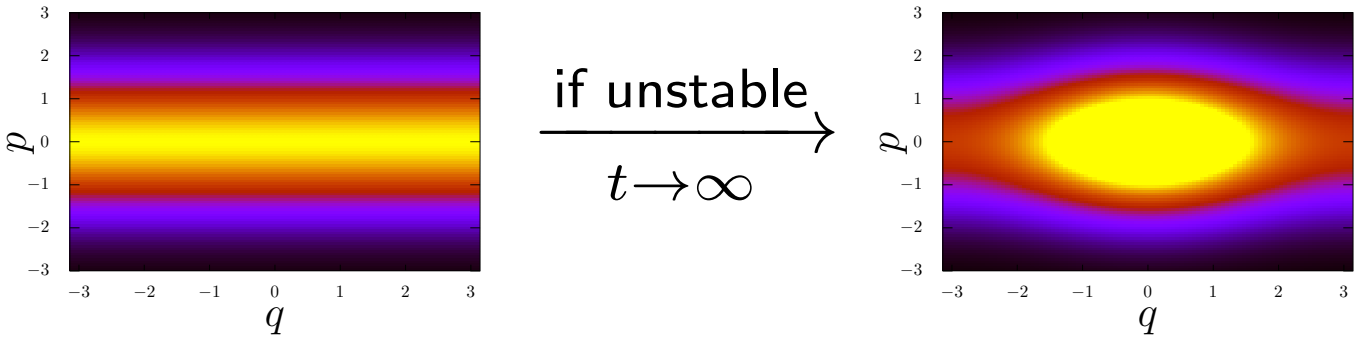

Final Cluster size C for unstable $F_{\rm ini}(p)$?

Knowns and Questions (K: coupling strength)

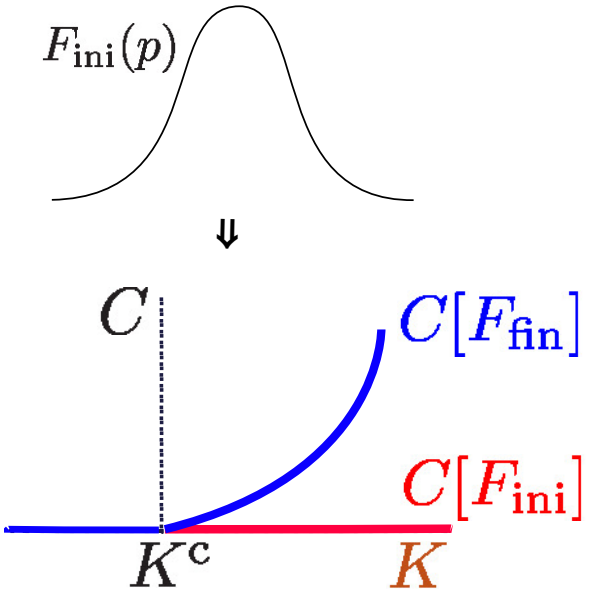

Continuous

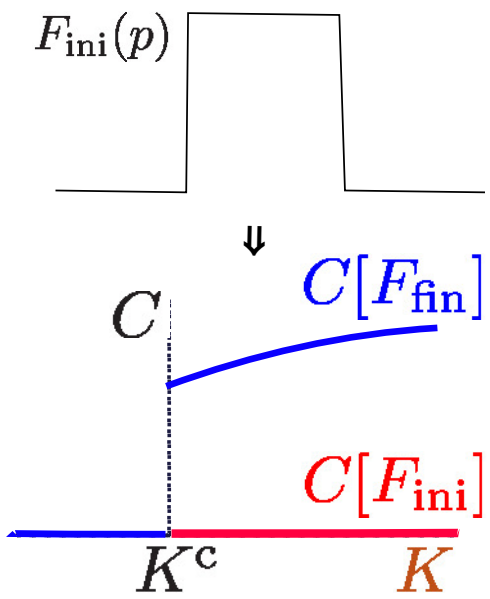

Discontinuous

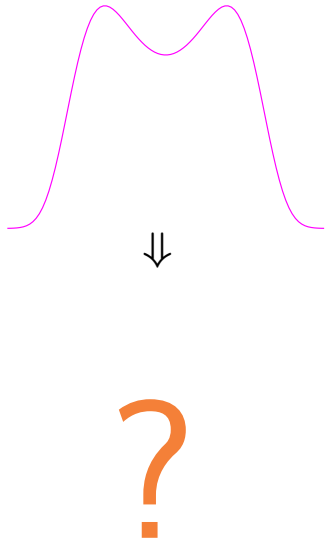

Q1 Where is the boundary of flatness?

Q2 For two-peak distributions?

Q3 How can we unify them?

We answer them via codim-2 bifurcation (tuning of 2 params)

Nice to meet you!

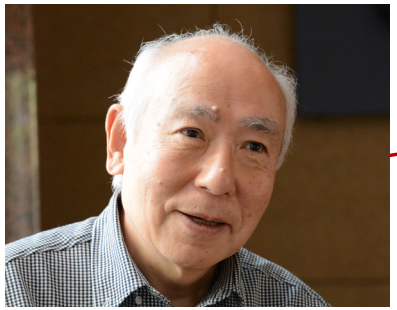

Yoshiki Kuramoto
(Nonlinear science)

UTokyo Nonlinear Physics Lab

Hiroshi Kori
(Synchronization etc.)

Ryota Kobayashi
(Data science etc.)

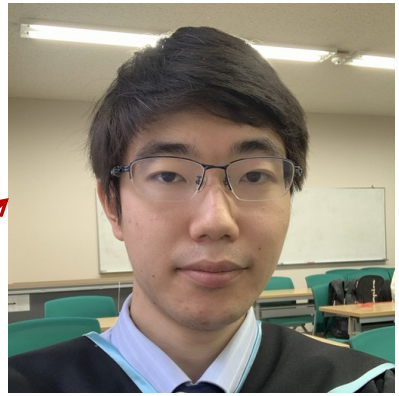

Taichi Yamamoto (M2)
yamamoto-taichi913@g.ecc.u-tokyo.ac.jp
Interests:
- Dynamics Reduction Theory
- Artificial Intelligence
- Koopman Operator
- Natural Computing

Supervisor Relation

Estimating Asymptotic Phase Function of Limit-cycle Oscillators using Gaussian Process Regression

Time series data → Phase function

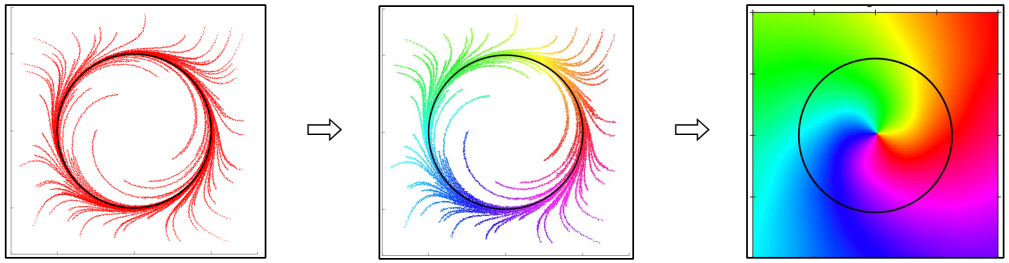

Hodgkin-Huxley model (4D)

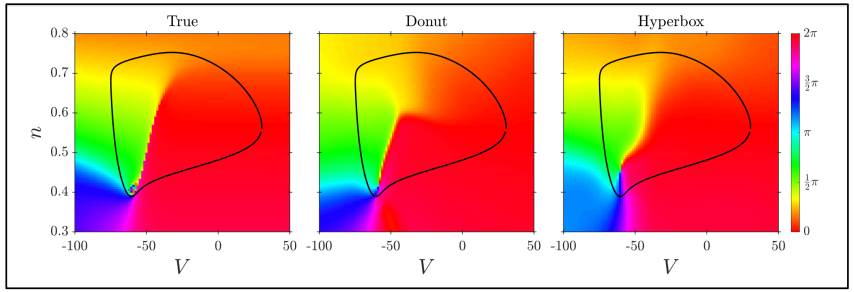

Robust against observation noise

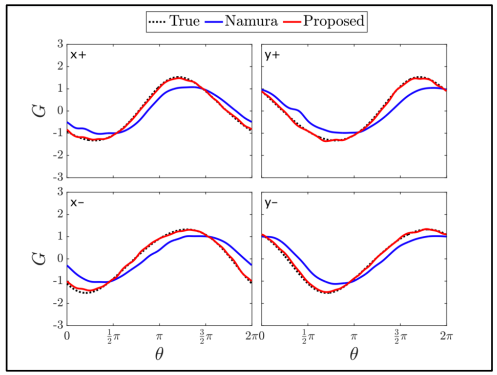

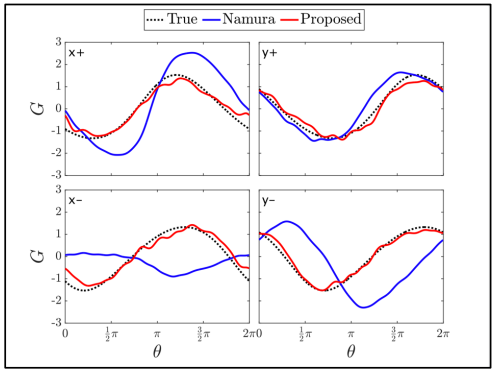

Predicting nonlinear phase response

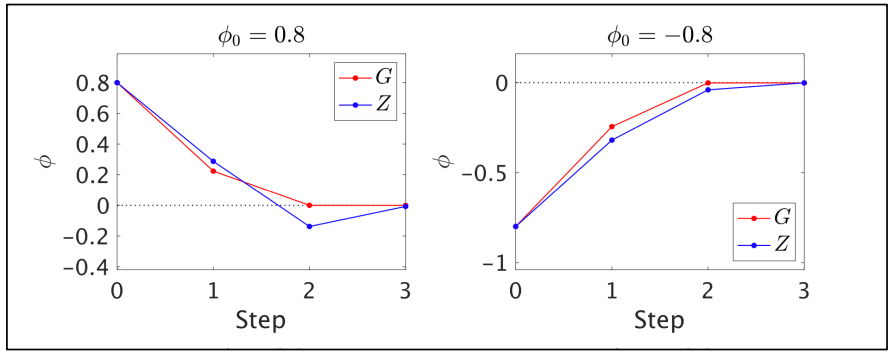

Attenuation of soliton by thermal vibration and anomalous heat transport in the FPUT lattice

Kazuyuki Yoshimura*, Masaki Takatsu（Tottori Univ, Japan.）

Fermi-Pasta-Ulam-Tsingou (FPUT) -β lattice

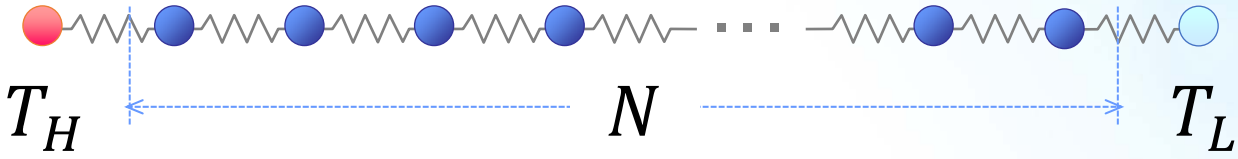

$$V(r) = \frac{1}{2}r^2 + \frac{\beta}{4}r^4$$

- Anomalous heat transport

$$\kappa \propto N^{\alpha},\ \alpha \simeq 0.4$$

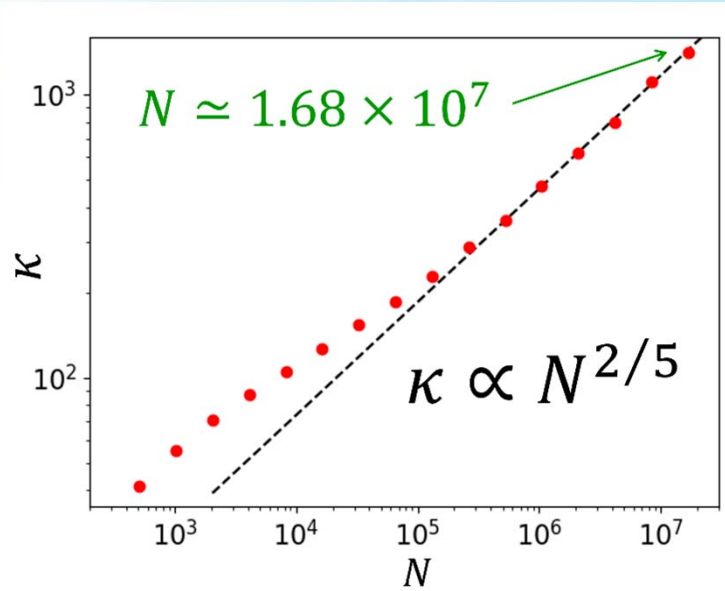

- **Mechanism**
- **Soliton dynamics**

M. Takatsu et al., J. Phys. Soc. Jpn. **93**, 053001 (2024)

Numerical experiment

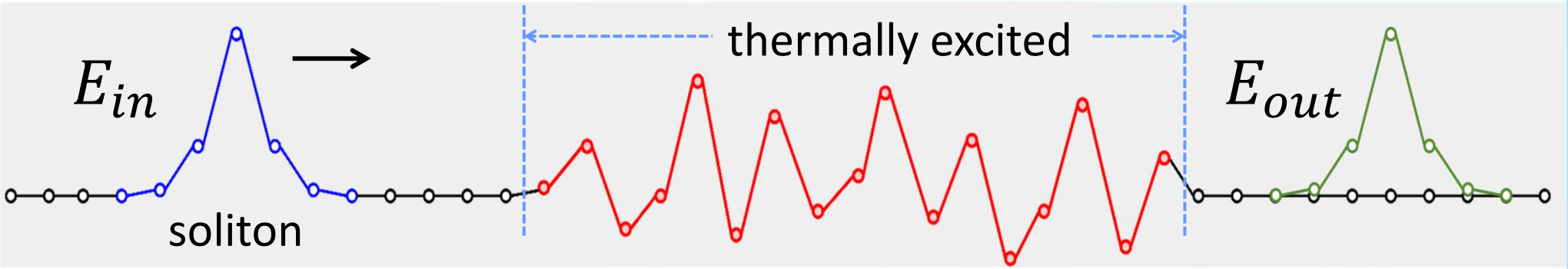

- **Power law of soliton energy decay rate:**

$$\frac{E_{in} - E_{out}}{E_{in}} \propto E_{in}^{c}\ , \quad \mathrm{c} \simeq 1.62$$

Soliton transport theory

- **Scaling law of anomalous transport:**

$$\kappa \propto N^{\alpha}\ , \qquad \alpha = 1 - \frac{1}{c} \simeq 0.383$$